JOURNAL OF GEOPHYSICAL RESEARCH, VOL. 104, NO. B8, PAGES 18,015–18,039, AUGUST 10, 1999

Three-dimensional velocity structure of Siletzia and other accreted terranes in the Cascadia forearc of Washington

Tom Parsons, Ray E. Wells, and Michael A. Fisher
U.S. Geological Survey, Menlo Park, California

Ernst Flueh
GEOMAR Research Center for Marine Geosciences, Kiel, Germany

Uri S. ten Brink
U.S. Geological Survey, Woods Hole, Massachusetts

Abstract. Eocene mafic crust with high seismic velocities underlies much of the Oregon and Washington forearc and acts as a backstop for accretion of marine sedimentary rocks from the obliquely subducting Juan de Fuca slab. Arc-parallel migration of relatively strong blocks of this terrane, known as Siletzia, focuses upper crustal deformation along block boundaries, which are potential sources of earthquakes. In a three-dimensional velocity model of coastal Washington, we have combined surface geology, well data, and travel times from earthquakes and controlled source seismic experiments to resolve the major boundaries of the Siletz terrane with the adjacent accreted sedimentary prism and volcanic arc. In southern Washington and northern Oregon the Siletz terrane appears to be a thick block (~20 km) that extends west of the coastline and makes a high-angle contact with the offshore accreted sedimentary prism. On its east flank the high-velocity Siletz terrane boundary coincides with an en echelon zone of seismicity in the arc. In northern Washington the western edge of Siletzia makes a lower-angled, fault-bound contact with the accretionary prism. In addition, alternating, east-west trending uplifts and downwarps of the Siletz terrane centered on the antiformal Olympic Mountains may reflect focusing of north-south compression in the northern part of the Siletz terrane. This compressional strain may result from northward transport and clockwise rotation of the Siletz terrane into the relatively fixed Canadian Coast Mountains restraining bend along the coast.

1. Introduction

Between 1991 and 1996, a series of controlled source seismic experiments were conducted in Oregon and Washington to determine the velocity structure of the seismically active Cascadia convergent margin [*Tréhu et al*., 1994; *Miller et al*., 1997; *Flueh et al*., 1997; *Parsons et al*., 1998]. Here we present a three-dimensional (3-D) seismic tomographic analysis of controlled source and earthquake travel time data aimed at resolving the large-scale geometry of the thick Eocene mafic basement of the Washington forearc and its relationship to the accretionary prism and volcanic arc (Plate 1). This basement underlies most of the forearc in Oregon and Washington and is known as the Crescent Formation in Washington and the Siletz River Volcanics in Oregon [*Snavely et al*., 1968]. Because of its mafic composition this forearc terrane, also known as the Siletz terrane, or "Siletzia" [*Irving*, 1979], is thought to be composed of strong crustal blocks that play an important role in forearc deformation [*Magill et al*., 1981; *Wells and Coe*, 1985; *Wells and Weaver*, 1993; *Tréhu et al*., 1994; *Stanley et al*., 1996]. Arc-parallel migration of these blocks in response to oblique subduction focuses upper crustal deformation and seismicity along block boundaries, which may be potential sources of earthquakes [e.g., *Wells et al*., 1998].

Along much of the Cascadia subduction margin, accreted sedimentary rocks are thrust beneath Siletzia along a major terrane boundary fault presumed to dip eastward beneath the Coast Range [e.g., *Tabor and Cady*, 1978a; *Snavely*, 1987]. Though this boundary is an important locus of strain accommodation, it is presently seismically quiet, and its earthquake potential is unknown. In the southwest Washington arc, however, the northwest trending Mount St. Helens and west Rainier seismic zones are thought to mark the eastern extent of Siletzia [e.g., *Stanley et al*., 1996; *Parsons et al*., 1998].

A detailed 2-D cross-section model was developed across southern Washington from controlled source data [*Parsons et al*., 1998] (Plate 2). This profile, while providing a relatively high-resolution image of the velocity structure across the margin, is only a single cross section and could not constrain the dip of the boundary between Siletzia and the accretionary complex because of the wide range of possible velocities in the metamorphosed accreted rocks at shallow depths. Possible interpretations of the velocity structure include landward or seaward dips (Plate 2). Multiple cross sections tied to the near-surface geology offer a better chance to constrain the dip. Thus one of the goals for conducting the 3-D study was to get a greater variety of ray paths through the accretionary and Siletz terrane rocks than were recorded along the 2-D profile.

Paper number 1999JB900106.

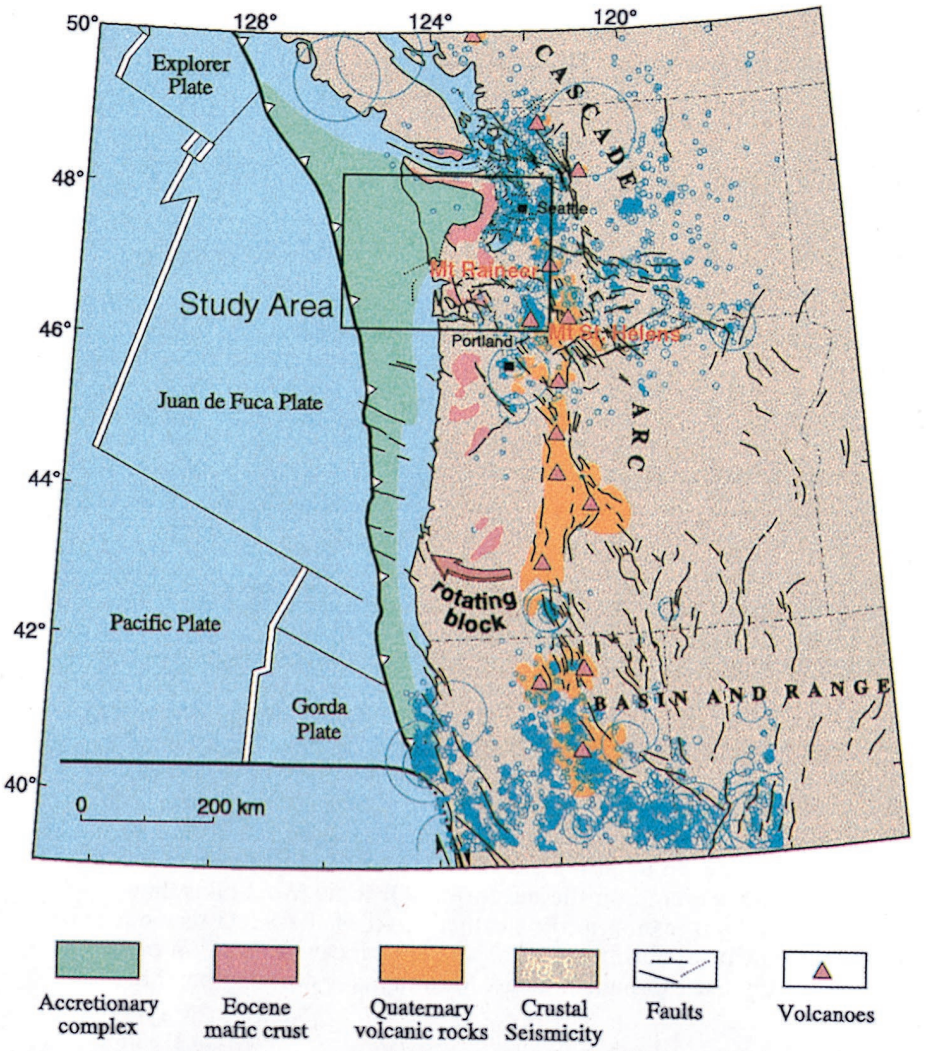

Plate 1. Major tectonic elements of the Cascadia subduction zone. There are important structural variations along the margin. The accretionary complex broadens progressively along the margin, reaching its widest point at the Olympic Mountains. Volcanic production is greatest in the central arc, where the seismicity rate is lowest.

The Cascadia subduction margin shows many along-strike tectonic variations such as accretionary-prism-width, seismicity rate, and volcanic production (Plate 1). Because of the important role that the Siletz terrane apparently plays in shaping the margin, defining the along-strike variation of its boundaries may provide some of the constraints needed to understand variations in the nature of deformation and earthquake potential along major upper plate structures in the Washington forearc.

1.1. Tectonic Setting

The Juan de Fuca plate subducts beneath North America at a rate of ~40 mm/yr on a N68°E azimuth [e.g., *DeMets et al*., 1990]. This oblique subduction has created a complex, geologically diverse, and potentially hazardous region, the Cascadia subduction zone and volcanic arc. No great Cascadia subduction zone earthquakes have been recorded in written history, and much of the region is relatively quiet seismically [e.g., *Dewey et al*., 1989]. However, global comparisons indicate that the Cascadia subduction zone has many characteristics in common with those that produce great interplate earthquakes; for example, young oceanic lithosphere subducts at shallow dip (similar to Central and South America, southwest Japan, and the Aleutians) [e.g., *Heaton and Kanamori*, 1984; *Heaton and Hartzell*, 1987]. Recent studies of the Holocene geologic record have shown consistent indications that great subduction zone and/or large upper plate earthquakes have affected the Washington coastal margin. Interpretation of geologic evidence (subsidence, tsunami deposits) along the coast has suggested that great earthquakes ($M > 8$) have occurred in the Cascadia subduction zone on a recurrence interval of hundreds of years [e.g., *Atwater*, 1996].

The Cascadia margin has had a long and complex history of deformation and volcanism resulting from Cenozoic oblique convergence between North America and subducting oceanic plates. In the Washington forearc, Cenozoic marine sedimentary rocks overlie Eocene basaltic basement of the Crescent Formation, which along with the correlative Siletz River Volcanics of Oregon, extend from the southern tip of Vancouver Island to the Klamath Mountains [*Snavely et al*., 1968; *Snavely and Wells*, 1996] (Plates 1 and 3). Sutured to North America at ~50 Ma, these voluminous (5–25 km thick) submarine and

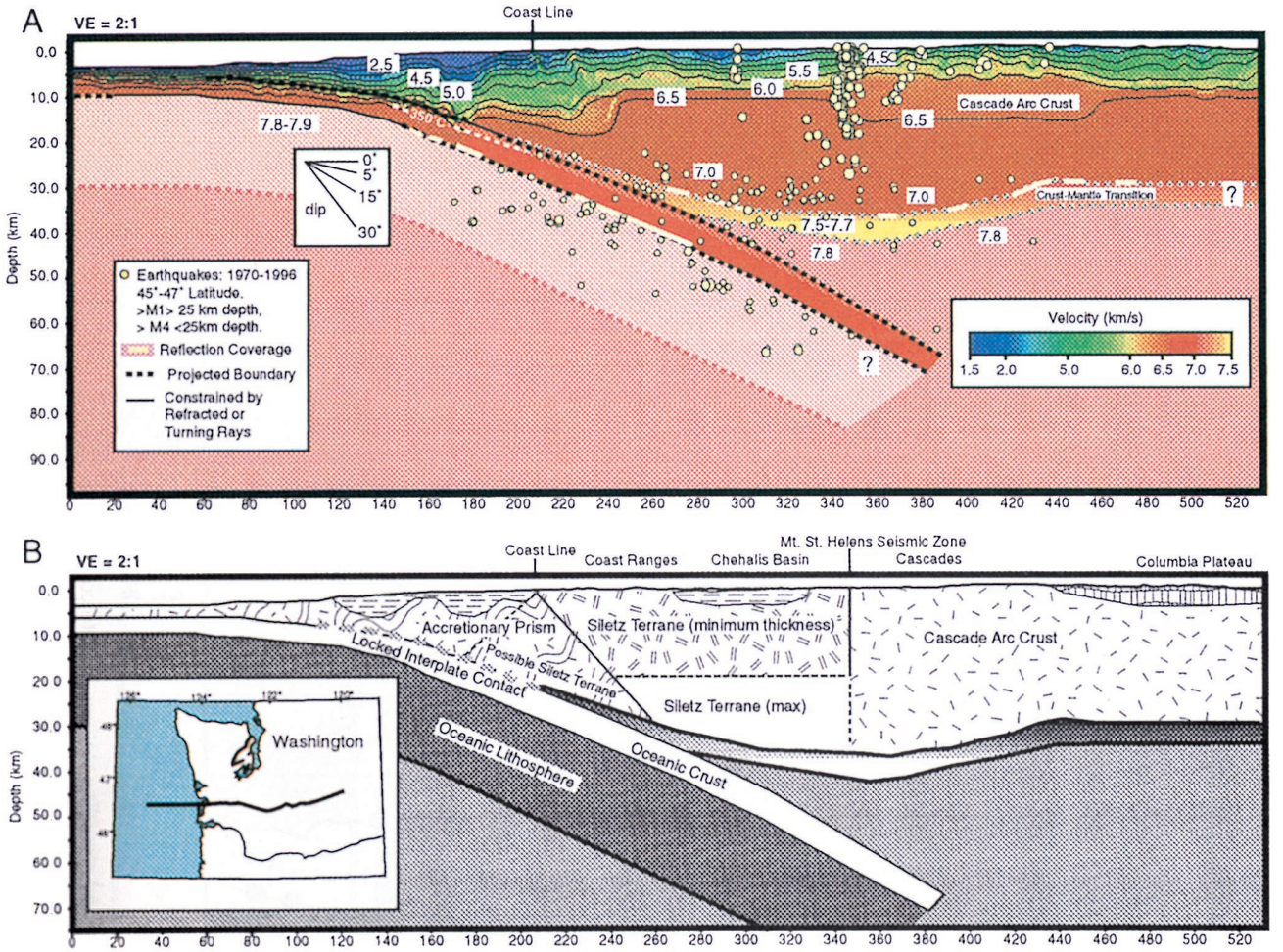

Plate 2. Interpreted cross-section velocity model along an east-west transect across southern Washington [*Parsons et al*., 1998]. From a single cross section like this it is difficult to resolve the Siletz-accretionary boundary. In this case it could either dip landward or seaward.

subaerial basalts may represent an accreted oceanic island chain [*Simpson and Cox*, 1977; *Duncan*, 1982] or a hot spot-generated continental margin rifting event [*Wells et al*., 1984; *Babcock et al*., 1992]. Paleomagnetic observations from Eocene Crescent Formation volcanic rocks in southwest Washington show significant (~20°–50°) clockwise rotations as does the Cascade arc, the result of oblique subduction of the Juan de Fuca plate [e.g., *Wells and Coe*, 1985; *Beck and Burr*, 1979]. Marine sedimentary rocks accrete against the Eocene volcanic rocks and have been exhumed since ~14 Ma in the Olympic Mountains, maintaining a steady state elevation since that time with erosion balancing tectonic uplift (M. T. Brandon et al., Late Cenozoic exhumation of the Cascadia accretionary wedge in the Olympic Mountains, NW Washington State, submitted to *Journal of Geophysical Research*, 1998).

Some knowledge about the subducted Juan de Fuca slab beneath the continent has been acquired through controlled source experiments, studies of regional earthquake hypocenters, and inversion of teleseismic arrival times for velocity structure. *Taber and Lewis* [1986] modeled a 9° dip on the Juan de Fuca slab beneath Grays Harbor. Farther south, at the latitude of Willapa Bay, *Parsons et al*. [1998] modeled a 12° dip on the slab beneath the margin (Plates 2 and 3). More broadly, beneath Washington, the Juan de Fuca plate appears to be arched along a southwest-northeast directed axis that crosses the northern Puget Sound [*Crosson and Owens*, 1987]. Interpretation of teleseismic travel time delays suggests a possible tear in the descending Juan de Fuca slab, with the dip angle steepening south of the Willapa Bay–Columbia River region [*Michaelson and Weaver*, 1986].

Seismic activity in western Washington is very low along the coast and increases inland, with hypocenters most abundant beneath the Cascade Range and Puget Sound (Plate 1). Deep earthquakes associated with the Juan de Fuca slab seem to mirror the distribution of upper plate earthquakes in the forearc. Two distinct north-northwest trending zones of shallow seismicity are associated with Mount St. Helens and Mount Rainier [e.g., *Stanley et al*., 1996] (Plate 1). Heat flow in coastal Washington is low (~20–50 mW/m^2), increasing to the east in the Cascade Range (~50–100 mW/m^2) and Columbia Plateau (~50 mW/m^2) [*Blackwell et al*., 1990].

1.2. Active-Source Seismic Experiments in Western Washington

In 1991 the U.S. Geological Survey (USGS) in collaboration with the University of Texas at El Paso, Oregon State University, the Geological Survey of Canada, the University of British Columbia, and the University of Wyoming collected a series of refraction profiles in Oregon and Washington [*Miller et al*., 1997]. Travel times from the northernmost refraction profile

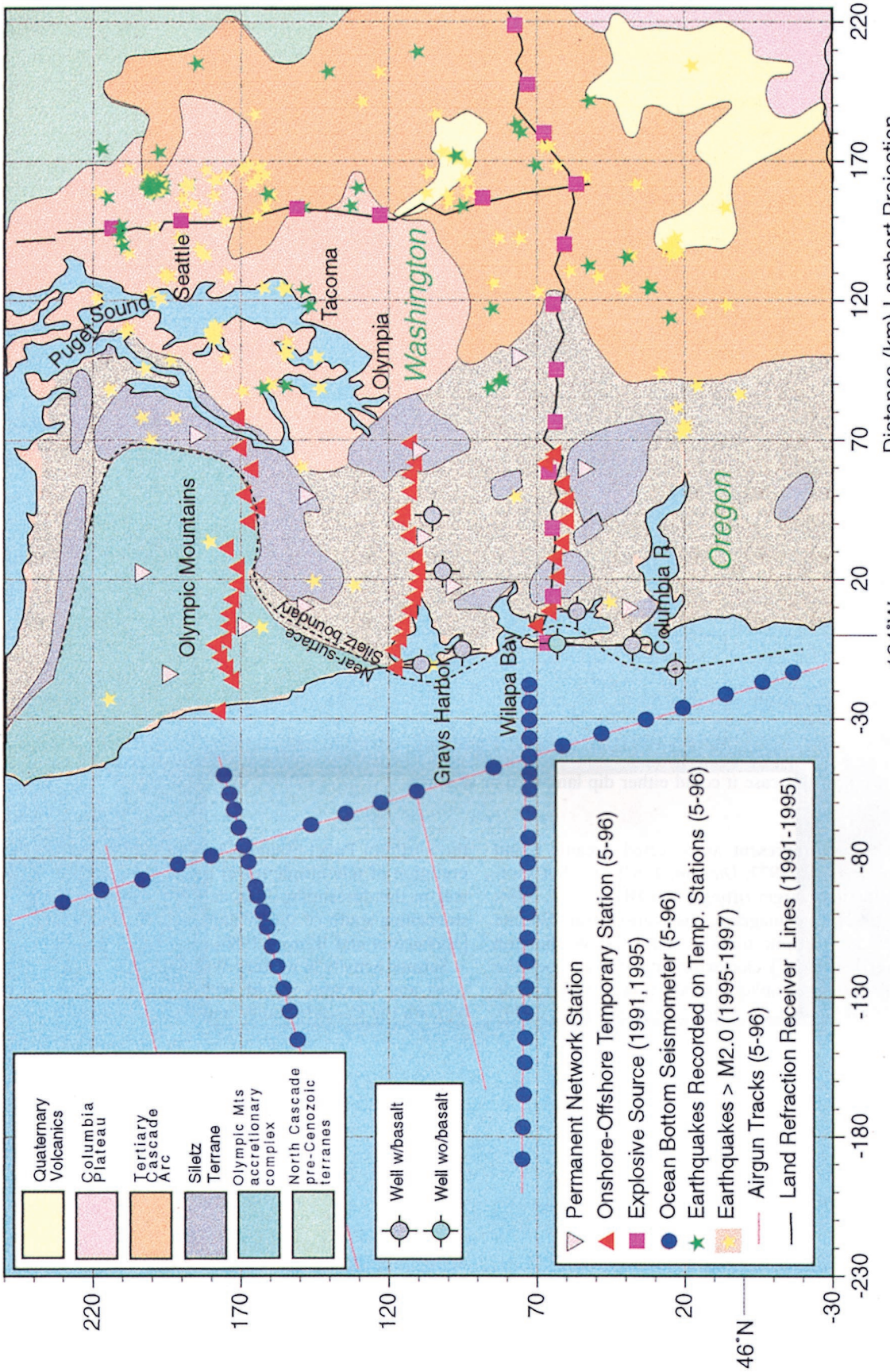

Plate 3. Locations of the controlled and earthquake sources and recording stations used to construct the 3-D velocity model. The generalized onshore geology is shown along with the locations of wells used [*McFarland*, 1979] to define the near-surface location of Siletzia shown by the dashed black line.

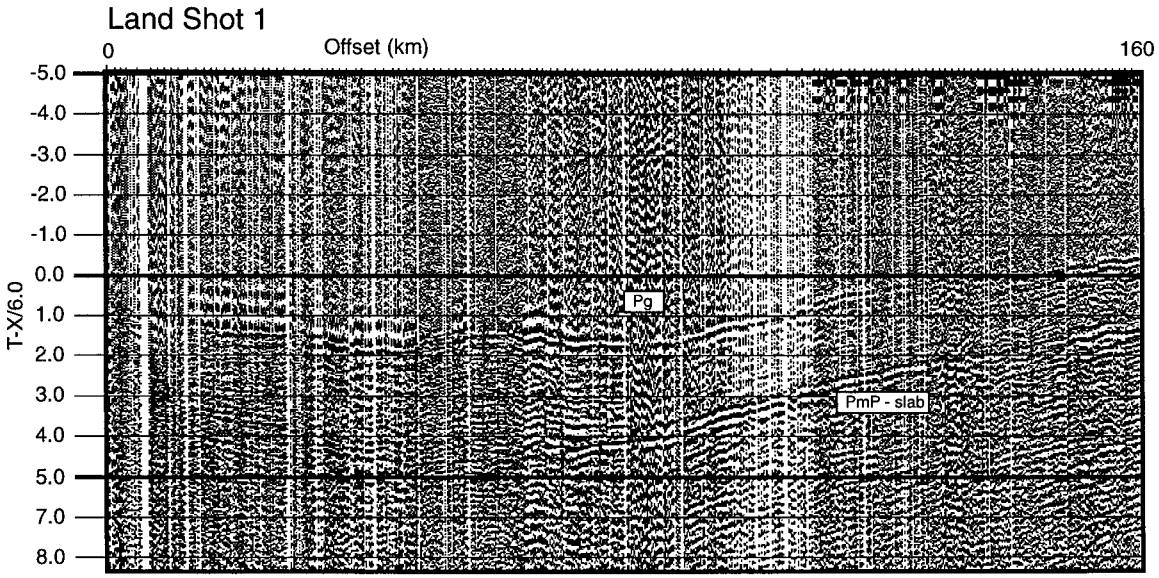

Figure 1. An example of explosive source data collected on land in southwest Washington showing the crustal refracted phase *Pg* that was used in the travel time inversion for velocity structure. Reflected phases such as the one shown from the Juan de Fuca slab were not applied.

that trended along the eastern side of Puget Sound (Plate 3) were applied in this study. This profile was composed of 10 large explosive sources detonated into a 465-channel land array (~600 m spacing) that was about 300 km long. We apply six usable sources from that study here (Plate 3).

In 1995, wide-angle seismic data were collected by the same collaborators along a 325-km-long east-west trending profile that crossed southern Washington from Willapa Bay to the Columbia Plateau (Plate 3) [*Parsons et al.*, 1998]. On that profile about 1500 instrument deployments were spaced at 200-m intervals, and 17 large explosive sources were recorded. An example of these data is shown in Figure 1. We apply 12 sources that fall within our study area from that profile here (Plate 3). The explosion data show images of the subducting slab (from reflections) and provide continuous first arrivals to 230-km offsets.

In 1996, the German research vessel, the *F. S. Sonne*, conducted an extensive investigation of the offshore Oregon and Washington margins in a joint GEOMAR-USGS effort [*Flueh et al.*, 1997]. A total of more than 14,500 air gun sources (50–150 m spacing) were fired offshore of Washington, with just over 6000 detonated along lines instrumented by a cumulative total of 53 ocean bottom recorder deployments on the seafloor (Plate 3). The balance of the air gun sources were fired for marine multichannel profiles. On land, 44 Reftek seismographs distributed (~5 km linear spacing) along three profiles (Plate 3) recorded all the air gun sources continuously. The ocean bottom and on-land profiles coincided along east-west profiles to provide continuous phase coverage across the margin and to enable comparison of structure from south to north (Plate 3). An example of air gun data recorded onland is shown in Figure 2. The onshore-offshore data show head waves traveling down the subducting slab as first arrivals in the near offsets and continental upper mantle refractions at longer offsets.

2. Travel Time Inversion for 3-D Upper Crustal Velocity Structure of Western Washington

2.1. Travel Time Data

A total of 69,251 *P* wave first-arrival travel times from controlled and earthquake sources were included in our velocity modeling. As can be seen in Plate 1, coastal Washington is seismically quiet; thus very few earthquake source arrival times were available for the coastal regions. The majority (67,898) of the travel times were from controlled sources, with only 1353 arrivals used from earthquakes (Figure 3). There are some advantages in applying primarily controlled sources; two of the free parameters of a simultaneous inversion, source location and origin time, are known, reducing uncertainties. However, all the controlled sources were located at the surface, limiting the deeper coverage that would result had more earthquake sources been available. For our velocity inversion we included only first arrivals, either *Pg*, the crustal refracted phase, or *Pn*, the upper mantle refracted phase. All controlled source seismic data were hand-picked on a computer screen display; we estimate picking errors to be 100 ms (one cycle at 10 Hz). Data examples are shown in Figures 1 and 2.

The limited set of earthquake travel times came from two data sets. The first group of earthquake source travel times was recorded by our temporary array deployed during April and May 1996 (Plate 3 and Figure 3). During this period we recorded ~300 earthquakes distributed across western Washington (green stars on Plate 3) including the $M = 5.4$ Duvall earthquake that occurred ~30 km east of Seattle and many of its aftershocks. We recorded only the vertical channel on our temporary network. A total of 267 high-quality arrivals that could be used in the velocity inversion were recorded on our 44 distributed stations. We defined a high-quality event as one recorded by at least five permanent network stations from the

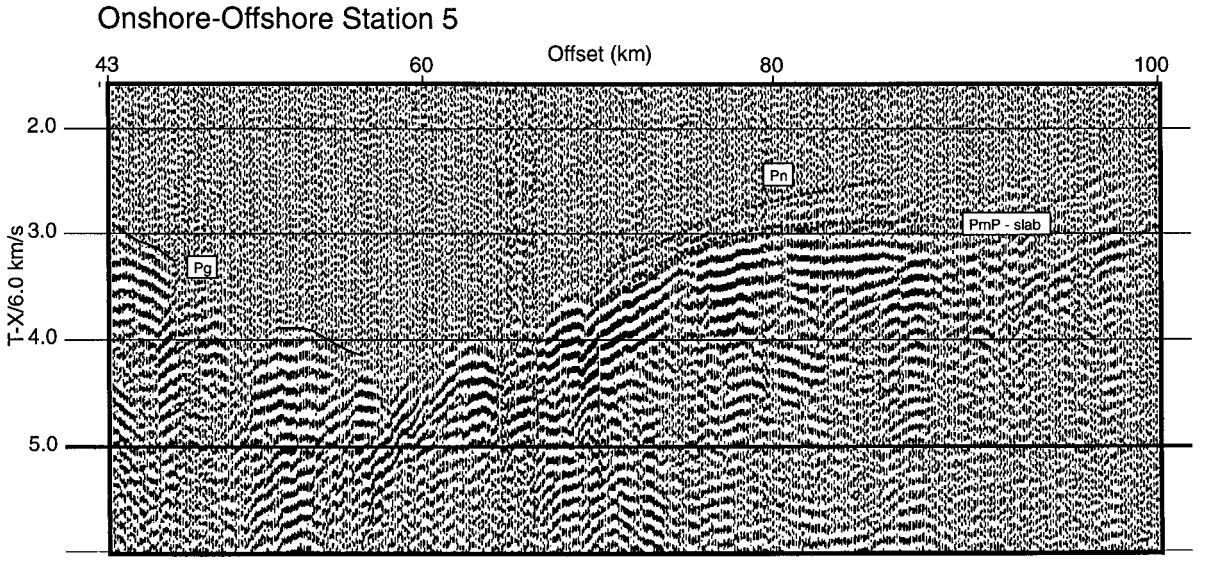

Figure 2. An example of air gun data collected on land showing the *Pg* phase and the upper mantle refracted phase *Pn* that were used in the travel time inversion for velocity structure.

Pacific Northwest Seismic Network (PNSN), and with an RMS error in location <2 km.

The second group of earthquake arrivals came from selected PNSN permanent stations that were located near the coast (pink triangles on Plate 3). We used data from a small group of well-located events (1995–1997, $M \geq 2.0$, yellow stars on Plate 3) recorded at 12 sites. The earthquake source regions in western Washington are dominantly the Puget Sound and Cascade areas; we thus used enough events to get a reasonably uniform sampling of travel paths through our 3-D model without clustering too many events in specific locations. The goal was to solve for the broad (25–50 km) scale velocity structure, thus adding large numbers of coincident sources would have added to computation times without significantly improving resolution.

2.2. Velocity Modeling Methods

We applied the 3-D tomographic technique of *Hole* [1992] modified to simultaneously invert for velocity, hypocenters, and origin times (hypocenters and origin times only for the earthquake data). This technique applies a finite difference solution to the eikonal equation (*Vidale* [1990]; updated by *Hole and Zelt* [1995]) to calculate first arrival times through a gridded slowness model. An iterative nonlinear inversion is performed as a backprojection along ray paths determined from the forward modeling step.

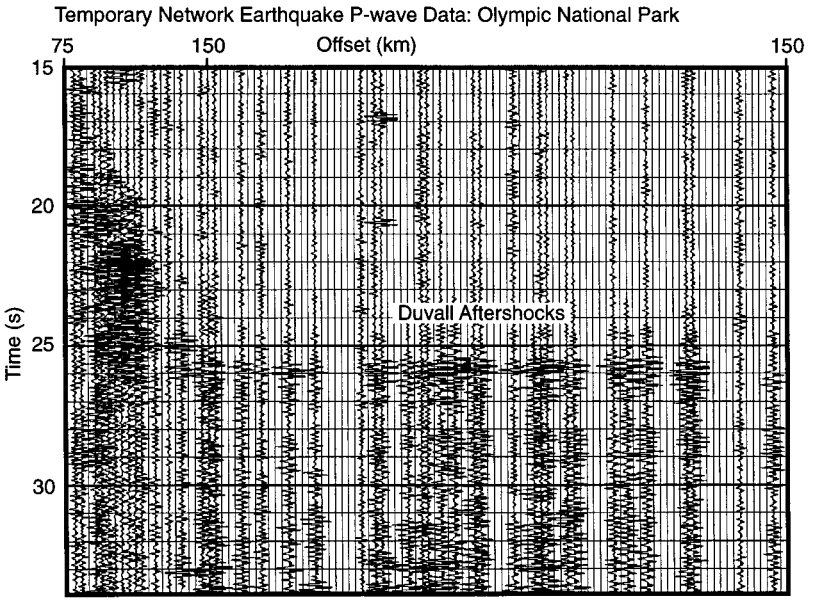

Figure 3. An example of local earthquake data collected on the vertical component showing the *Pg* phase. Since many of the events recorded are aftershocks from the Duvall earthquake, they are not plotted at an equal offset scale; if they were, most of the Duvall events would be plotted on top of each other. Instead, the events are plotted at a variable offset scale.

We chose a larger 3-D volume to model than that containing the targeted coastal region where the Siletz terrane meets accreted sedimentary rocks so that we could include important seismic source regions such as the offshore airguns and the seismically active Puget Sound region (Plate 3). Our choice of a large model volume created regions of relatively sparse ray coverage. Therefore, as always, the choice of a starting model was important in guiding the final model. We extrapolated a smoothed version of the detailed 2-D model of *Parsons et al*. [1998] parallel to the margin to generate a 3-D starting model. In many cases we observed head waves from the dipping Juan de Fuca slab as first arrivals from the offshore air guns; thus having the approximately correct slab structure in the starting model allowed for the proper treatment of these arrivals. Starting models were discretized into grids of 2.5-km cells; we used relatively small grid cells to ensure accurate calculation of ray paths along short source-receiver offsets.

We compiled travel time picks for controlled (Figures 1 and 2) and earthquake (Figure 3) sources for each receiver as a function of their 3-D spatial source locations and inverted them for 3-D velocity structure. Initial hypocenter locations and origin times of earthquakes were input as determined by the PNSN. A spatial smoothing filter was applied to the models between velocity and source parameter iterations. Early iterations were conducted that applied very broad smoothing filters (up to 100 km) and limited source-receiver offset ranges to solve the shallowest parts of the velocity model first. Subsequent iterations were conducted that included greater source-receiver offsets and progressively smaller smoothing filters.

The earthquakes used in this study were initially located with a 1-D velocity model; thus a degree of coupling between hypocenter location and the velocity structure derived from earthquake traveltimes is unavoidable and could cause significant errors in the resolved velocity models [e.g., *Thurber*, 1993], especially in areas where controlled sources were absent. To reduce such errors, hypocenters and origin times were relocated while controlled source locations and times were held fixed. The events were relocated between velocity iterations (mean relocation was 0.28 km). See *Hole* [1992] for full details on the travel time inversion algorithm.

2.3. Resolution

Resolution in tomography depends on three properties of the problem. The signal band width, the source-receiver distribution, and the velocity structure itself. For crustal scale experiments the signal wavelengths are typically much smaller than the gaps in ray path coverage (as they are in this study (2–20 Hz)). Three approaches are usually adopted to investigate resolution in tomographic problems. The simplest is a hit count analysis. In this analysis the number of rays sampling a given cell is examined to identify regions of good coverage and poor coverage. The second approach to resolution analysis is the construction of synthetic tests using the data distribution [*Humphreys and Clayton*, 1988]. The synthetic test may be an attempt to construct point spread functions or may be an attempt to reconstruct the major features of the model simultaneously. The third common method of resolution analysis is the use of the resolution matrix of linear inverse theory. Typically, the diagonals of the resolution matrix are displayed, and a certain value is chosen to indicate good resolution. The resolution matrix is a construct well suited to the study of linear problems. However, the extension of this tool to nonlinear problems is always questionable, particularly when the solution is approached iteratively [*Shaw and Orcutt*, 1986].

Each of the above resolution diagnostics depends on the velocity structure used to construct the resolution measures. Quantitatively connecting a hit count, synthetic test, or resolution matrix with the actual accuracy of the reconstructed image is not straightforward. A combination of these resolution indicators can provide some intuition into the resolving power of the data. We have chosen to use a backprojection and thus do not construct a formal resolution matrix. We instead show the hit count to illustrate the seismic ray coverage and use checkerboard tests to estimate the degree of uniqueness of the solution. Our estimates of spatial and relative velocity resolution based on the checkerboard tests vary with depth, and we thus report them individually as we show slices from the 3-D velocity model. The checkerboard tests were conducted by calculating synthetic travel time picks between all the source and receiver positions through a model of 50×50 km columns, each with alternating increasing velocity gradients that were 0.5 km/s different at all depths (Plates 4–8). Additionally, we alternated vertical gradients at various depths (to create checkerboards in cross section) to test our resolution of horizontal velocity boundaries. We tested only resolution of increasing velocity gradients within column elements.

An important aspect to tomography is to scale the smoothing dimensions appropriately to the input travel time data. On the basis of the distribution of seismic sources and receiver stations we sought to resolve velocity anomalies $\geq$50 km across in the lateral dimensions and $\geq$10 km thick in the vertical dimension. We thus applied a 25-km-wide by 5-km-high smoothing filter during the final iteration, which yielded an RMS travel time misfit of 0.31 s. A smaller RMS misfit could be achieved but would require reducing the model smoothness below the appropriate scale for the input data coverage, resulting in an artificially detailed velocity model.

2.4. The 3-D Velocity Structure of Western Washington: Observation

We show and discuss horizontal slices from the 3-D model volume at 5 km depth intervals that are windowed around the regions of best data coverage (Plates 4–8) as illustrated by the accompanying hit count plots. We show also an associated checkerboard test for each velocity slice. All reported depths are below sea level.

2.4.1. The 2.5 km depth. Our model had limited coverage at this depth (Plate 4a). Many of the velocity features shown are actually inherited from vertical smoothing of anomalies resolved deeper in the model. The 2.5-km model slice does show fairly uniform velocities of about 4.5 km/s in the Coast Ranges, where there is good coverage. The accompanying checkerboard test result (Plate 4b) demonstrates the relatively poor resolution in the uppermost layer. Some of the checkerboard pattern was recovered, though vertical smoothing of deeper, better resolved parts of the test model may have influenced that. Because of the limited coverage at shallow depths away from the controlled source transects, we failed to image the low-velocity Seattle and Tacoma basins (beneath Puget Sound) [*Lees and Crosson*, 1990; *Symons and Crosson*, 1997] except very near to the 1991 land refraction profile (Plates 4a and 3).

2.4.2. The 7.5 km depth. The seismic ray coverage improves with depth into the middle crust and is relatively good in the center of the model at 7.5 km (Plate 5a). Offshore, fairly

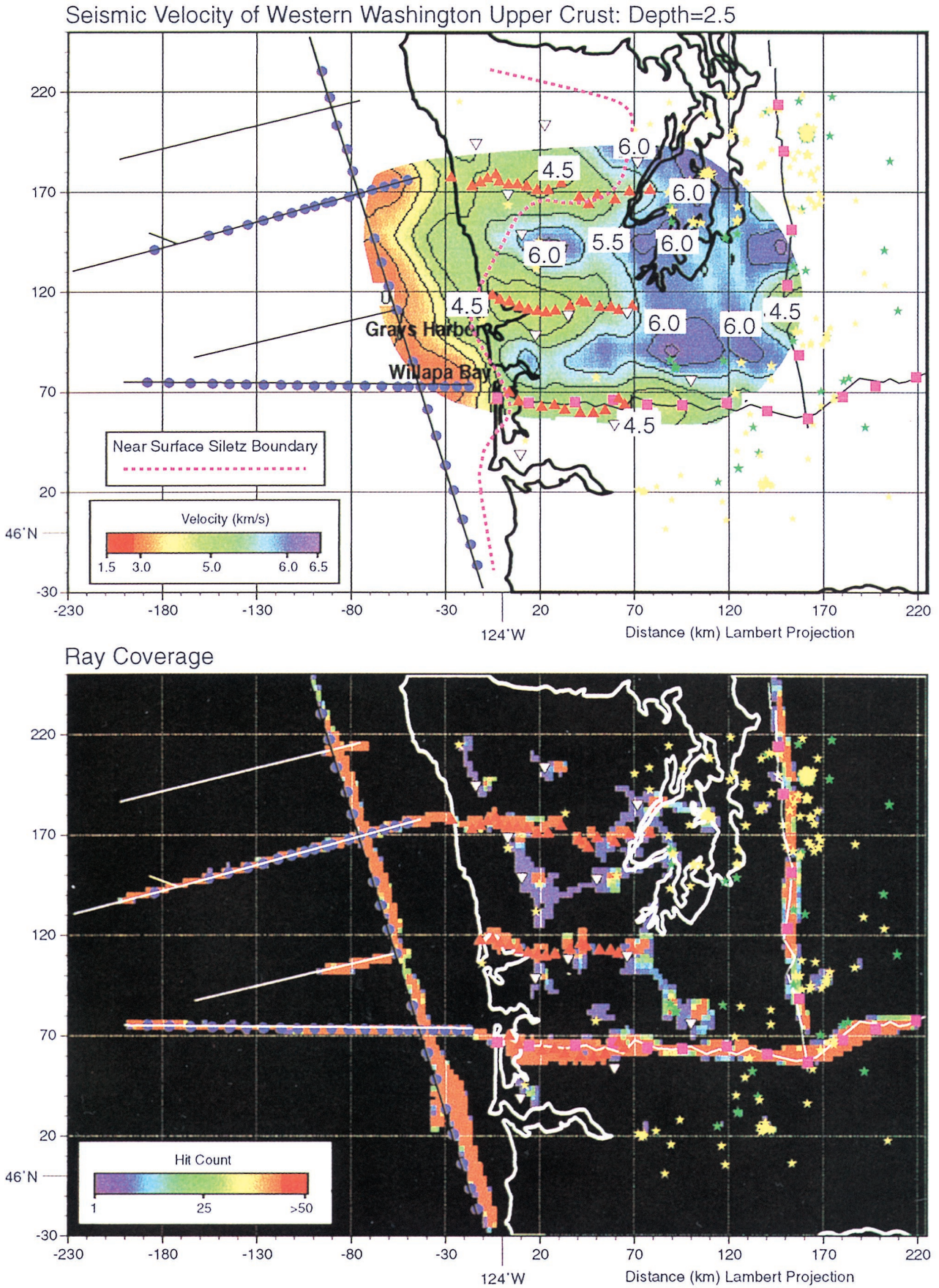

Plate 4a. Horizontal slice from the 3-D velocity model volume taken from 2.5 km below sea level. See text for full discussion of the model slice and resolution test. See Plate 3 legend for description of symbols.

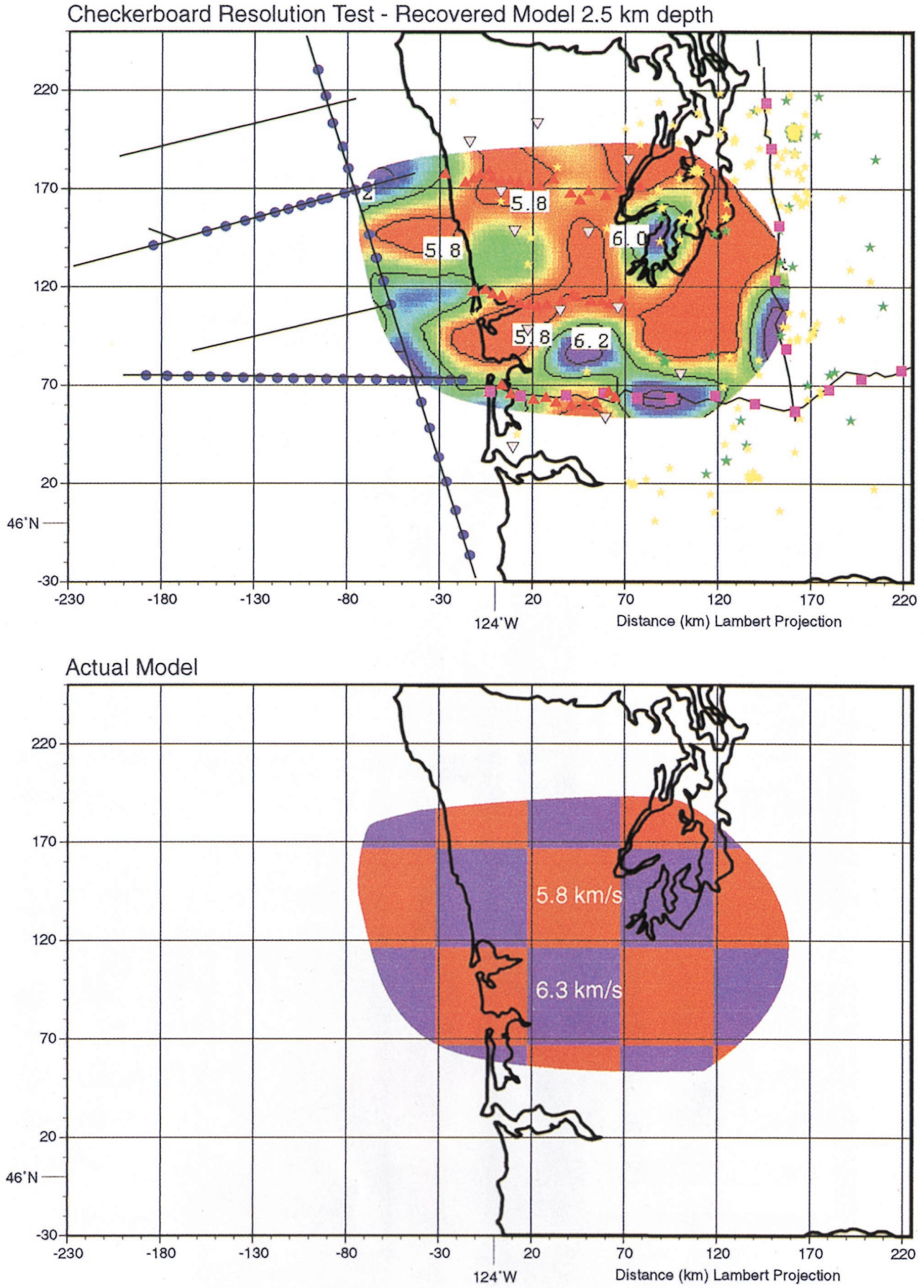

Plate 4b. Results from a checkerboard resolution test (2.5 km depth) with the recovered model shown above the input model.

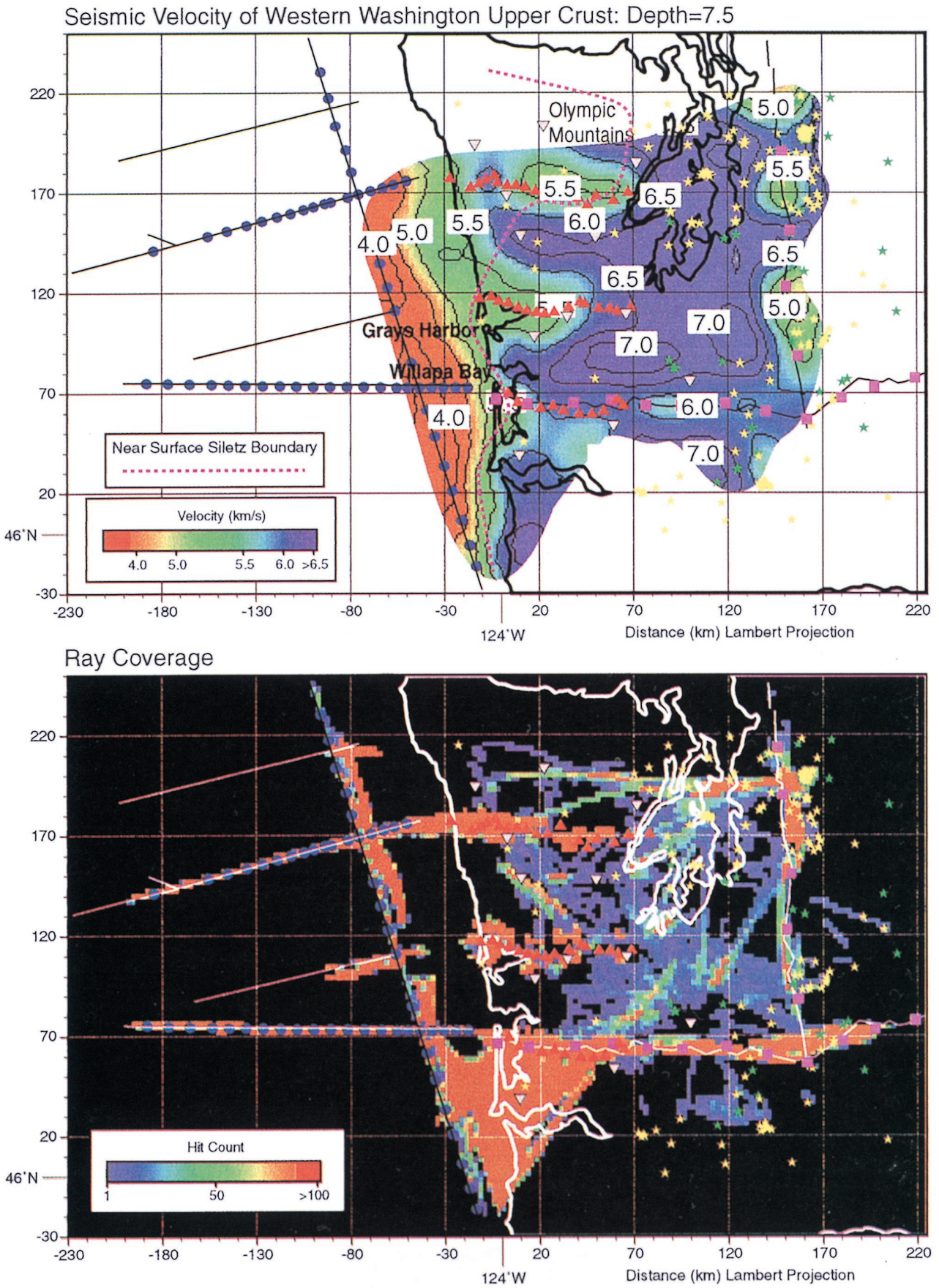

Plate 5a. Horizontal slice from the 3-D velocity model volume taken from 7.5 km below sea level.

low velocity rocks (3.5–5.5 km/s) are imaged. Onshore, a large body of relatively high velocity rocks (>6.0–6.5 km/s) occupies much of the crust, extending from near the coastline to the east of Puget Sound (Plate 5a). The high-velocity rocks are present at the coastline in northern Oregon and southern Washington; farther north along the coast, the high-velocity rocks retreat inland at Grays Harbor and again in the Olympic Mountains. An apparent pattern of alternating east-west trending high- and low-velocity bodies is evident along the coastline.

The resolution test at 7.5 km depth shows reasonably good recovery of the checkerboard pattern (Plate 5b), with edges resolved to within ±10 km laterally and relative velocities resolved to an average of ±0.15 km/s. Because of the broad lateral smoothing applied to the velocity model we cannot resolve dips very accurately. A ±10 km lateral shift at 7.5 km depth implies a ±55° change in dip between a surface outcrop and the associated velocity anomaly. Thus at this depth, only very high angle versus very low angle velocity boundaries can be discriminated.

Our observation of an alternating pattern of high and low velocities along the coast looks at first glance to be a result of a coverage bias in that the three east-west onshore-offshore profiles (where coverage tends to be best) are associated with lower velocities (i.e., Plate 5a). However, the two southern lines were located in basins, and the northernmost line was located on the accretionary rocks of the Olympic Mountains, where velocities are expected to be lower. South of the Olympic Mountains, the high velocities were modeled from travel times to PNSN stations. Immediately south of Grays Harbor, the high velocities may not extend all the way to the coast as shown, given that there is a hole in the coverage there (Plate 5b). However, the high velocities modeled farther south near the coastline around the mouth of the Columbia River are better constrained (Plate 5b). The generally high velocities modeled north and south of Grays Harbor are not artifacts from the starting model; instead, they result from the addition of the PNSN data. If the PNSN data are excluded from the inversion, the observed velocity pattern is one of lower velocities smeared across the coastal areas. The addition of the PNSN stations reduced the overall RMS misfits, thus we think that the higher-velocity areas are not a result of any systematic timing errors associated with the earthquake travel times.

It is possible that some vertical smearing of very low velocities near the surface could be influencing the velocity image where we observe low-velocity anomalies because we have poor coverage in the upper 2 km, though the persistence of low velocities associated with these regions through the 12.5 km depth range (see subsequent discussion) exceeds the vertical smoothing dimension (5 km), passes through the best covered parts of our model, and includes rays from sources and receivers away from the areas at the surface that correspond with the lower-velocity regions.

2.4.3. The 12.5 km depth. At 12.5 km depth an overall northeast trend of the west edge of higher-velocity rocks (>6.5 km/s) from Willapa Bay in the south to Puget Sound in the north becomes clear. An embayment of lower-velocity rocks (<6.0 km/s) at Grays Harbor is still evident at 12.5 km depth (Plate 6a). To the east, high velocities drop off dramatically along a north trending boundary that corresponds roughly to the west Rainier seismic zone.

Lateral spatial resolution at 12.5 km depth is comparable to that at 7.5 km depth (±10 km) (Plate 6b), though the recovered relative velocity resolution is a little worse at about ±0.2 km/s. The checkerboard pattern recovery continues to be better along the western part of the model window than along its east side.

2.4.4. The 17.5 km depth. The pattern of higher (>6.5 km/s) and lower (<6.5 km/s) velocity rocks at 17.5 km depth resembles that at 12.5 km depth (Plate 7a). The western edge of the higher-velocity block continues to have a northeast trend. Higher-velocity rocks are observed in the offshore region beginning at this depth. Spatial (±20 km) and velocity resolutions (±0.3. km/s) are reduced relative to shallower slices (Plate 7b).

2.4.5. The 22.5 km depth. The relatively consistent observation of a higher-velocity body of rocks onshore as compared with the offshore region between 2.5 and 17.5 km depth is lacking at this depth (Plate 8a). Instead, fairly uniform 6.5–7.0 km/s rocks are continuously distributed. We conducted vertical and horizontal resolution tests to establish if we could continue to observe the onshore high-velocity anomaly at 22.5 km depth. The checkerboard pattern was shifted from that in layers above to test the lateral resolution while eliminating the possibility that the recovered pattern might incorporate some smoothing from layers above where there was better seismic ray coverage (Plate 8b). We found that we could recover the checkerboard pattern to some extent and could estimate the lateral resolution to be ±15–20 km, with ±0.2 km/s resolution in velocity. Thus, if there was a lateral velocity contrast such as was observed at all other depths in the model, we should be able to resolve it at 22.5 km depth.

2.5. The 3-D Velocity Structure of Western Washington: Interpretation

The primary goal in generating the 3-D velocity model is to identify the boundary between Siletzia and the sedimentary rocks accreted against it. Siletzia in western Washington is made up of the Crescent Formation and is composed of massive and pillowed basalt flows and is cut by diabase dikes [e.g., *Tabor and Cady*, 1978a]. In contrast, where exposed in the Olympic Mountains, the sedimentary rocks accreted against Siletzia are primarily sandstones and mudstones of increasing metamorphic grade from east to west [e.g., *Tabor and Cady*, 1978a; *Brandon and Calderwood*, 1990]. Thus it is expected that Siletzia rocks are much higher velocity than the accreted sedimentary complex. To interpret the actual boundary between these rocks, we need to know their velocity-depth functions; while some data exist for the Siletz terrane [*Parsons et al*., 1998; N. I. Christensen, unpublished data, 1998], little is known about the accretionary complex. We can, however, gain insight from a global compilation of velocity measurements that shows a fairly narrow transition from metamorphosed sedimentary rocks into metamorphosed mafic igneous rocks [*Christensen and Mooney*, 1995]. Given the coarse smoothing applied to our 3-D model and resulting velocity resolution (~±0.2 km/s), such an approach provides reasonable guidelines for interpretation. In Figure 4 the results of *Christensen and Mooney* [1995] are summarized graphically; the metasedimentary rocks fall below a velocity range with depth from ~6.1 to 6.4 km/s, while the mafic intrusive rocks tend to fall above that curve, with the exception of unmetamorphosed basalt. Where exposed in Washington, Siletzia rocks are zeolite to prehnite-pumpellyite facies [*Tabor and Cady*, 1978b]. We thus interpret the velocity range between 6.0 and 6.5 km/s as containing the Siletz-accretionary boundary, which takes into account our average ±0.2 km/s lateral velocity resolution (Figure 4). In Washing-

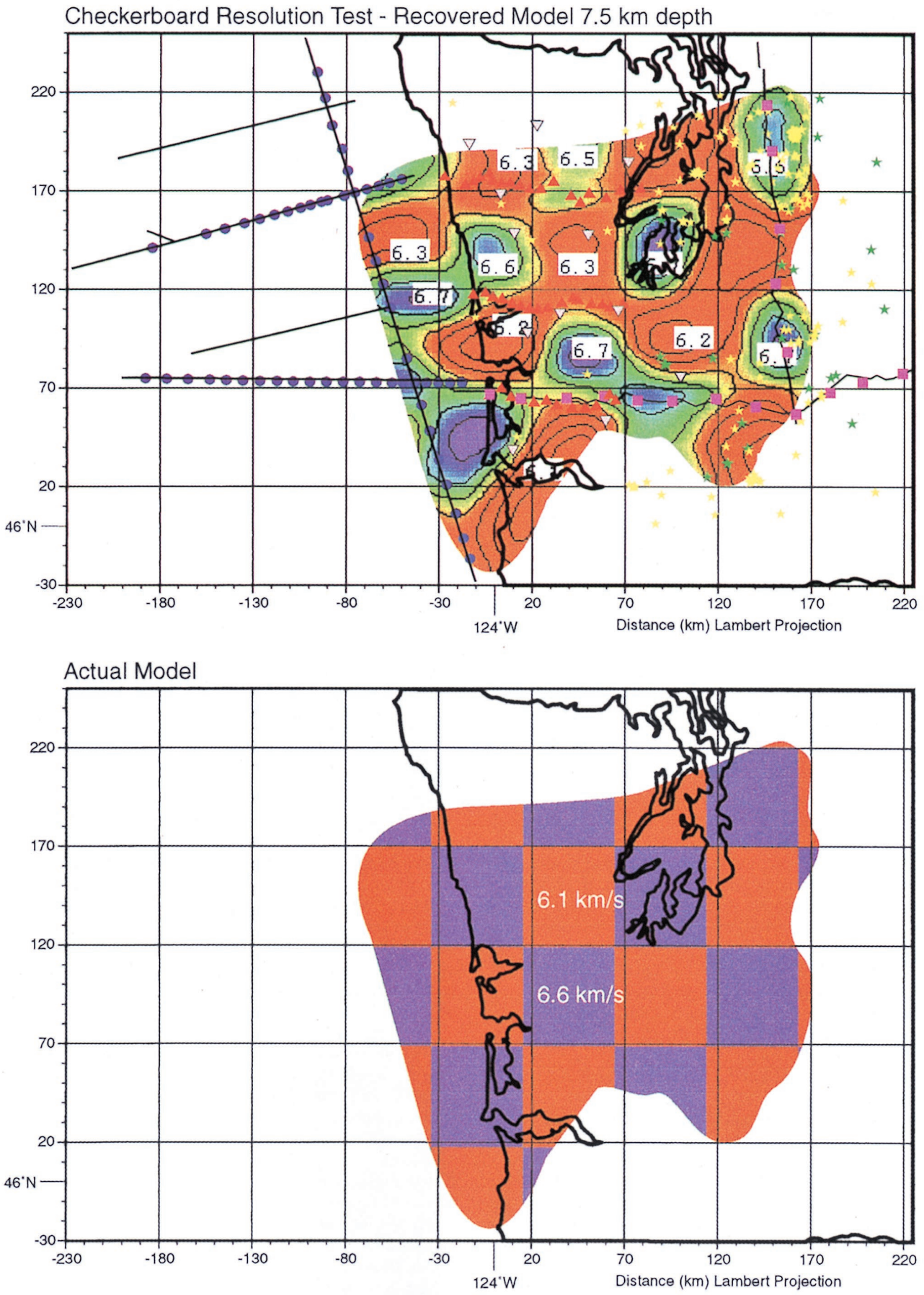

Plate 5b. Results from a checkerboard resolution test (7.5 km depth) with the recovered model shown above the input model.

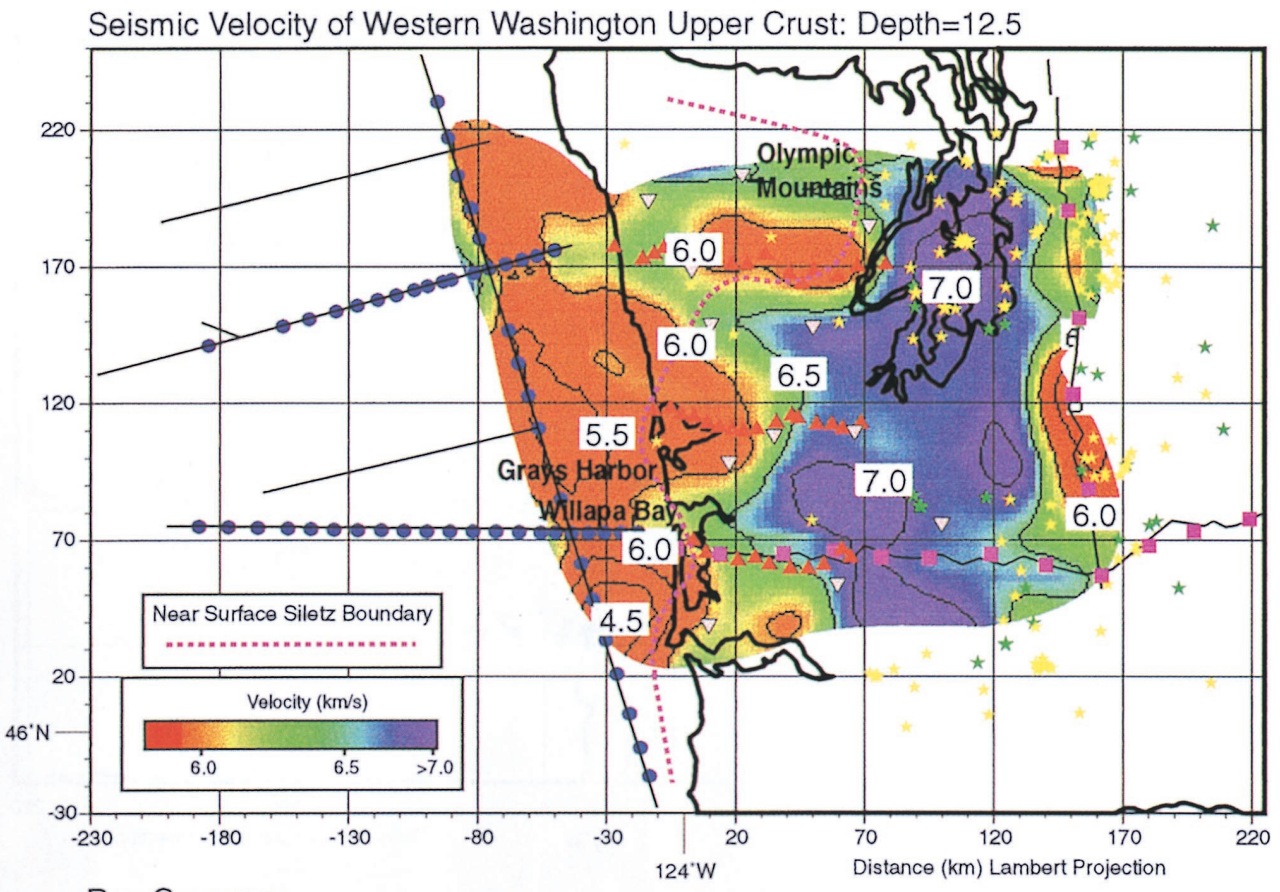

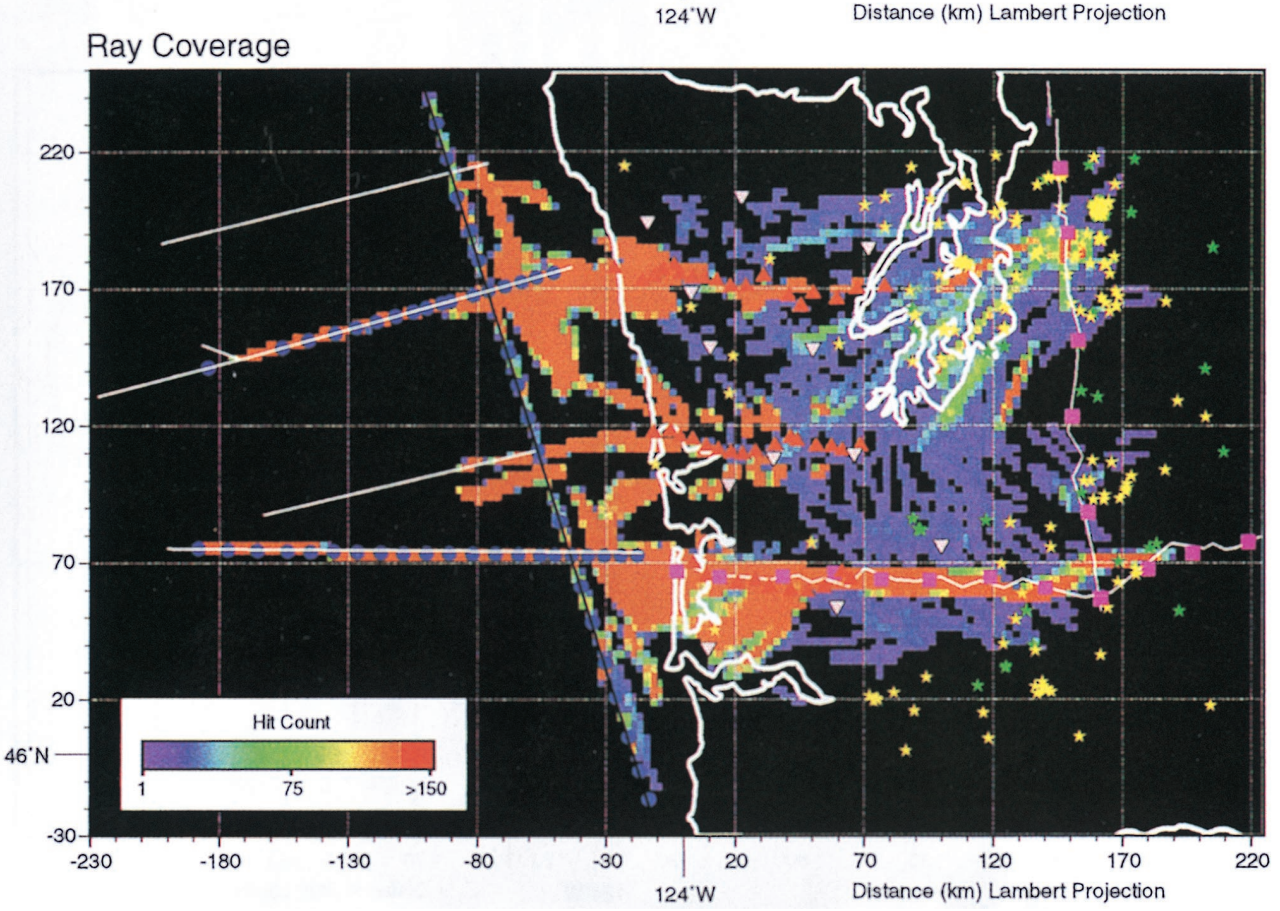

Plate 6a. Horizontal slice from the 3-D velocity model volume taken from 12.5 km below sea level.

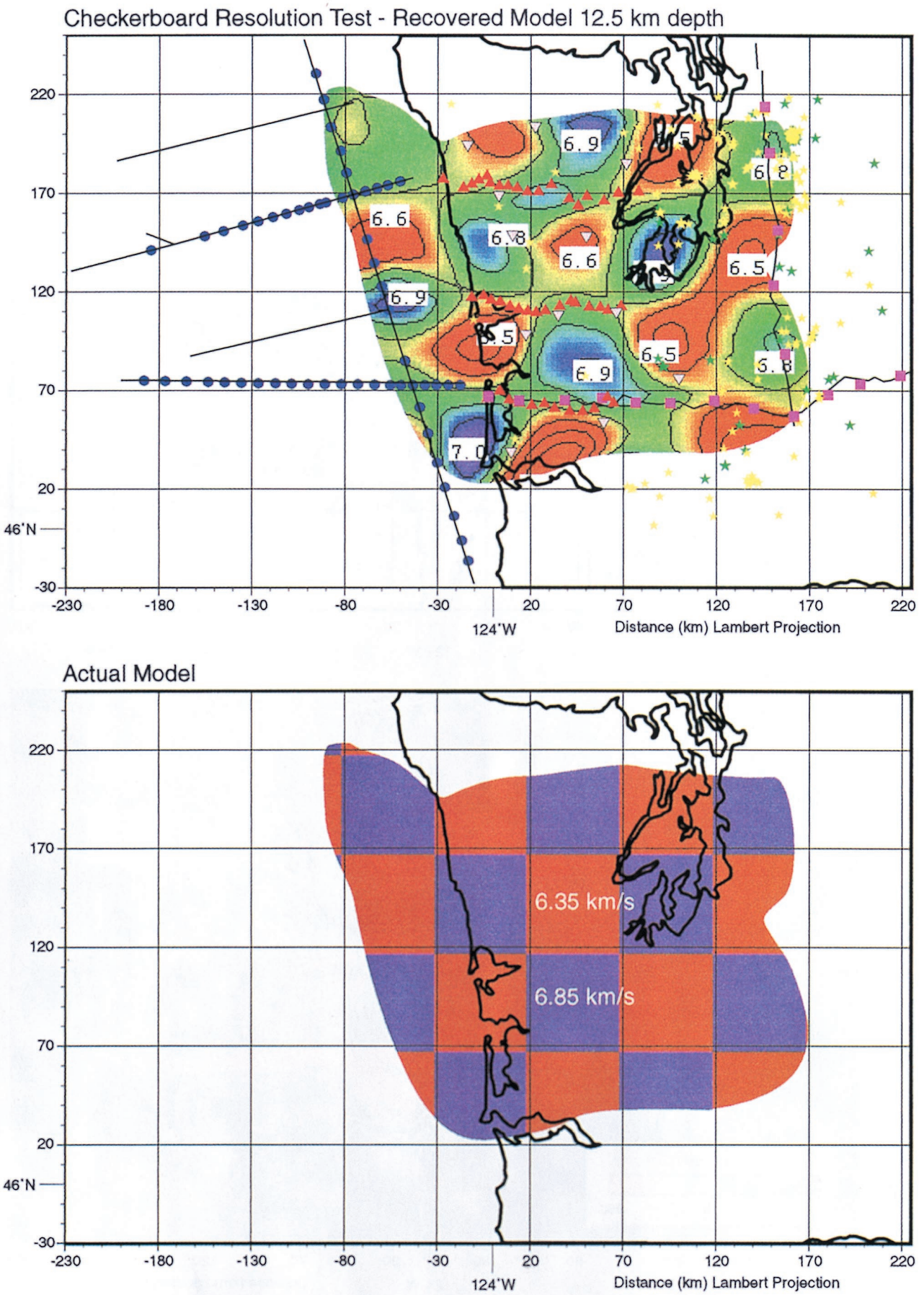

Plate 6b. Results from a checkerboard resolution test (12.5 km depth) with the recovered model shown above the input model.

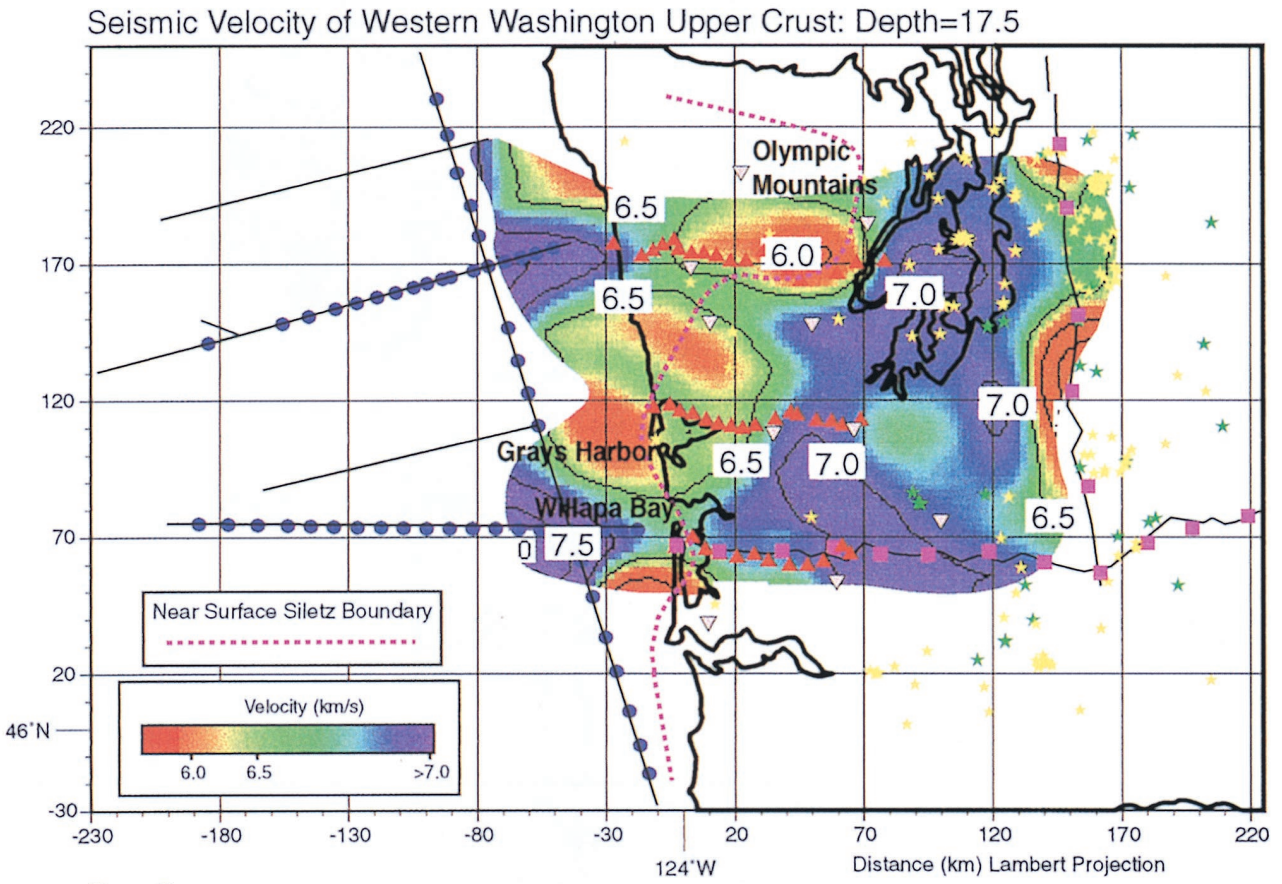

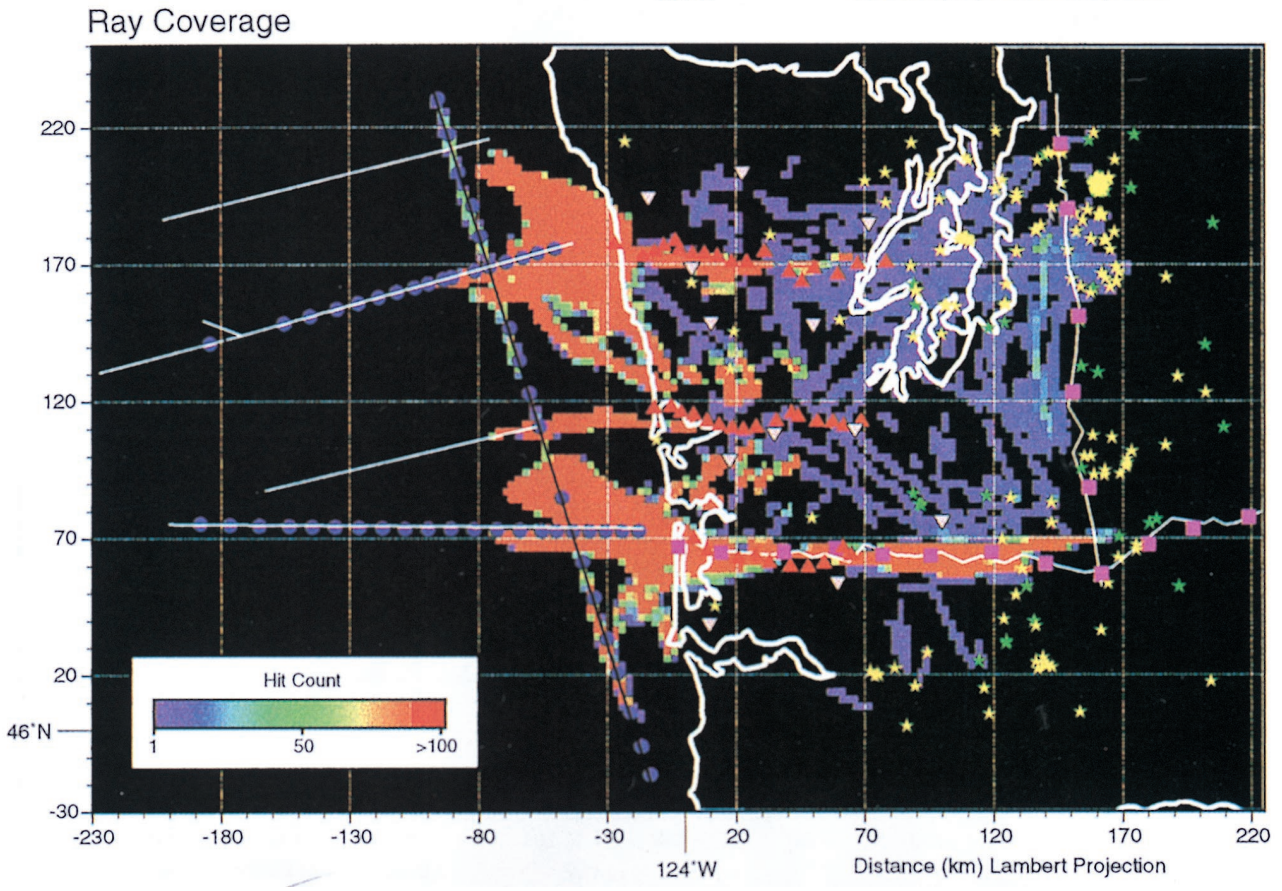

Plate 7a. Horizontal slice from the 3-D velocity model volume taken from 17.5 km below sea level.

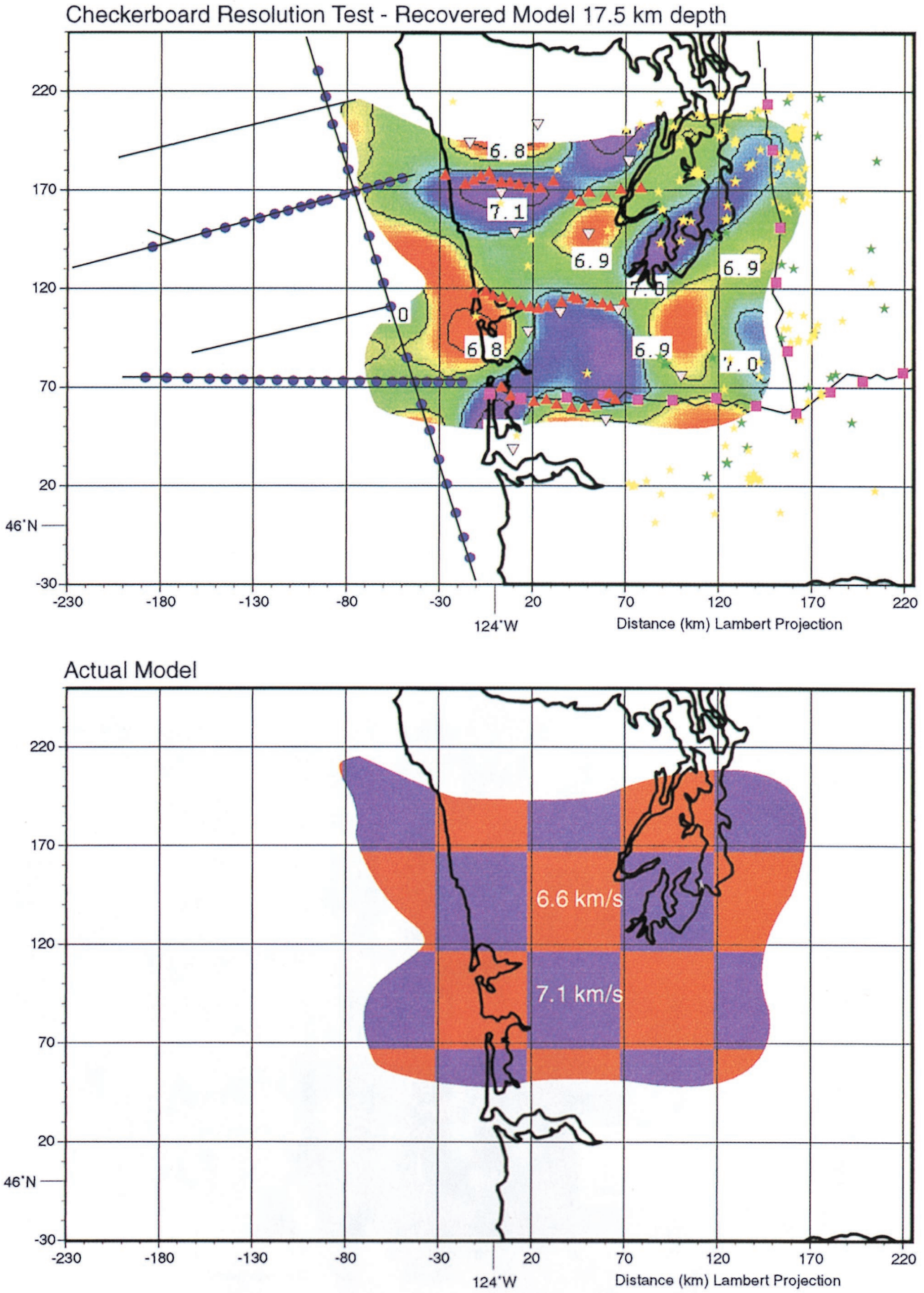

Plate 7b. Results from a checkerboard resolution test (17.5 km depth) with the recovered model shown above the input model.

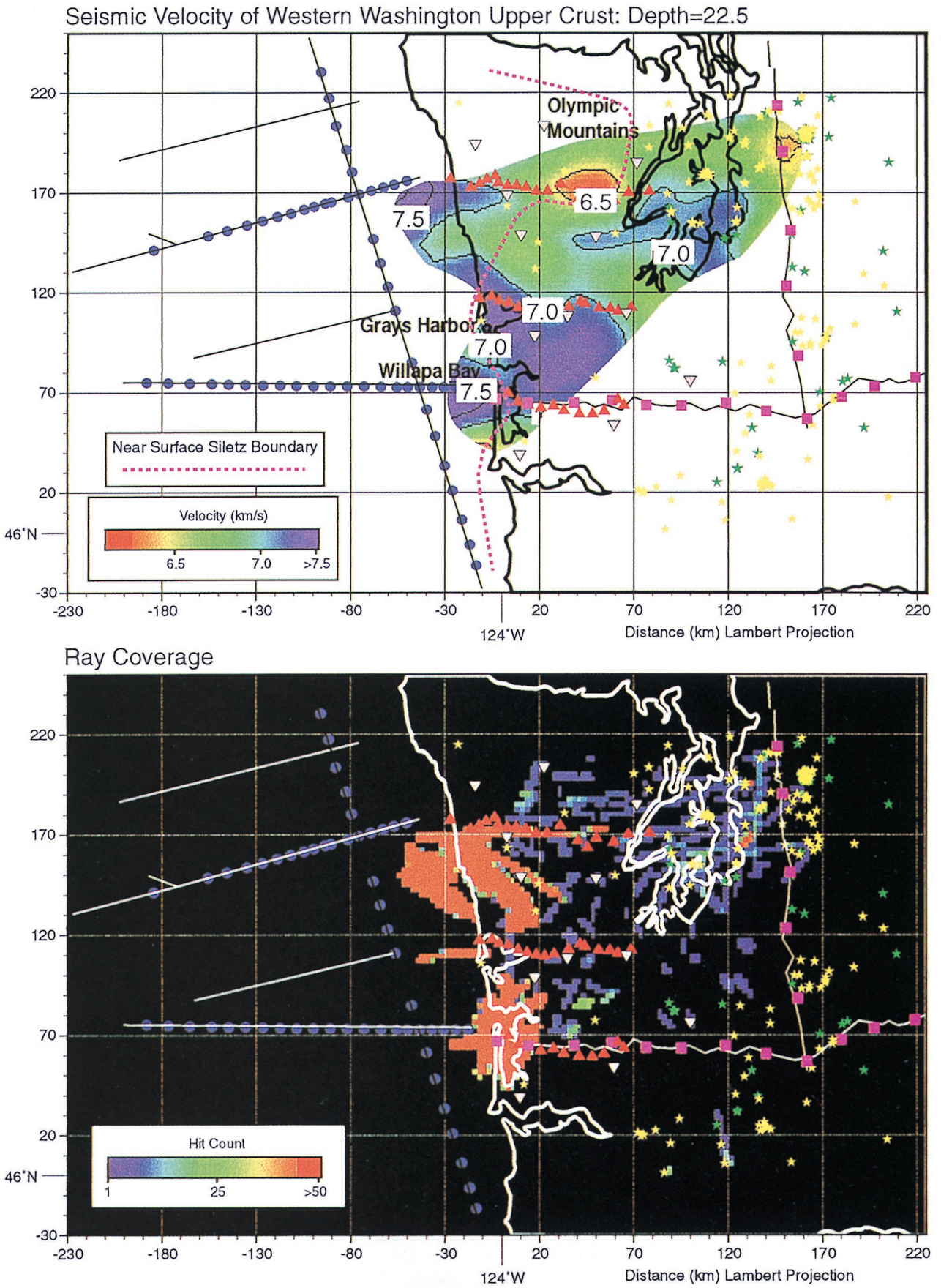

Plate 8a. Horizontal slice from the 3-D velocity model volume taken from 22.5 km below sea level.

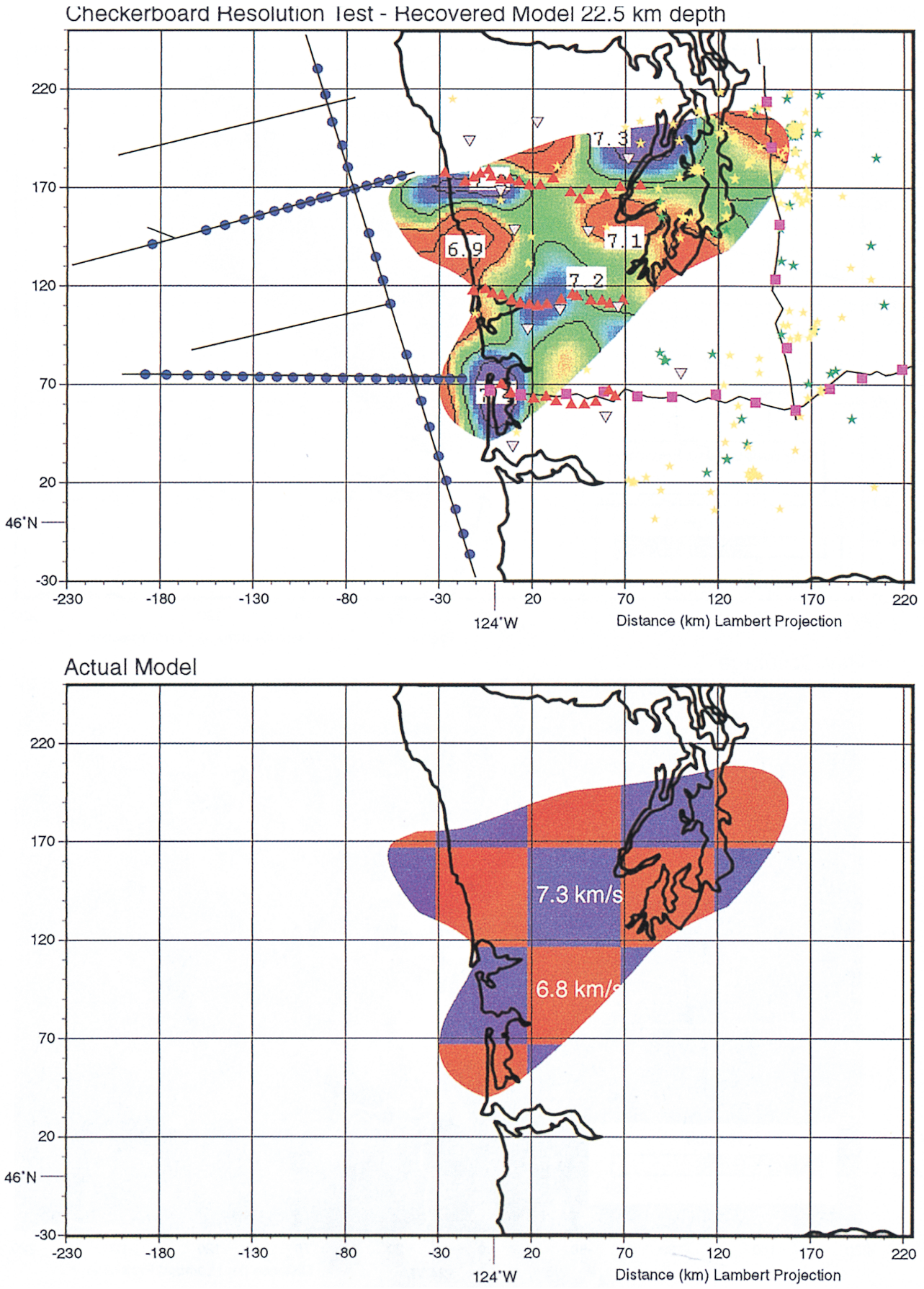

Plate 8b. Results from a checkerboard resolution test (22.5 km depth) with the recovered model shown above the input model.

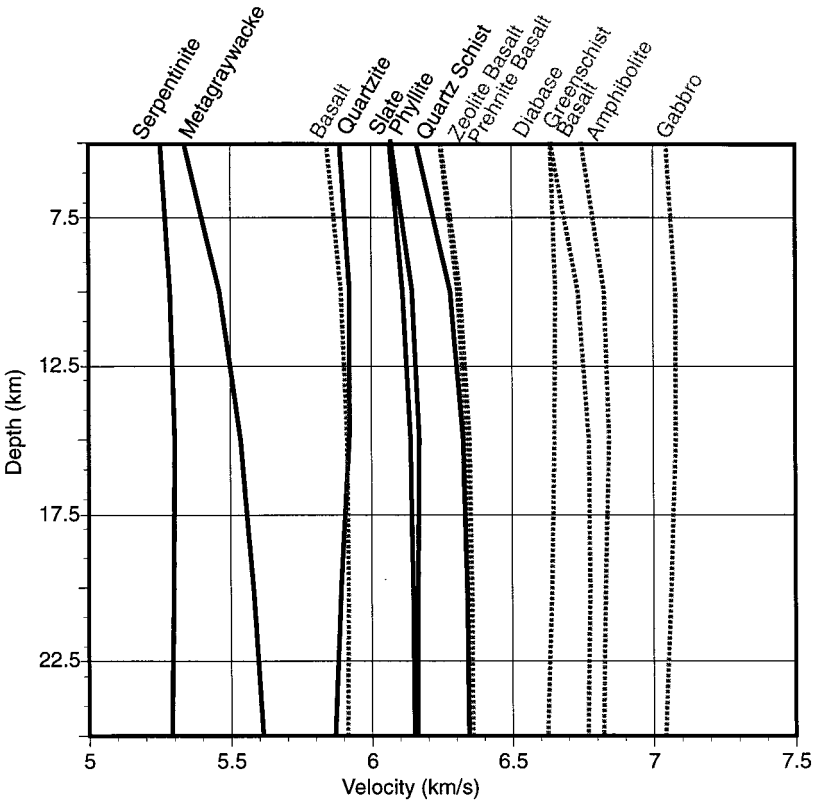

Figure 4. Velocity-depth curves from global averages of hundreds of measured samples of the major classifications of sedimentary, metamorphic, and igneous rocks [*Christensen and Mooney*, 1995] of likely composition and grade to be found in the upper 25 km of the Cascadia subduction zone [e.g., *Best*, 1982]. Given the ±2 km/s lateral velocity resolution of the 3-D velocity model, we interpret from the velocity depth curves that the Siletz-accretionary complex boundary is contained in the velocity interval between 6.0 and 6.5 km/s.

ton, no ultramafic rocks are exposed at the surface in outcrops of Siletzia, but on Vancouver Island the sequence is floored by gabbros [*Massey*, 1986]. We therefore interpret the highest velocities (~7.0 km/s) at depth as a gabbro layer near the base of the Siletz terrane. We make geologic interpretations of the velocity anomalies identified on slices from the 3-D model in section 9.

2.5.1. The 7.5 km depth. High-velocity rocks at depth match fairly closely with the surface outcrops of Siletz rocks and well data [*McFarland*, 1979] (Plates 3 and 5a). We thus interpret the large body of high-velocity rock that occupies most of the crust onshore as the Siletz terrane (Plate 5a) (specifically, the Crescent Formation of the Siletz terrane). We interpret the lower-velocity anomalies west of the Siletz terrane and offshore as accreted sedimentary rocks. At depth, high velocities are seen at varying offsets to the east of the near-surface contact between Siletzia and accreted sedimentary rocks (Plate 5a). The near-surface and 7.5-km-deep contacts are nearly coincident in northern Oregon and southern Washington, while we observe a significant eastward shift north of Willapa Bay (Plate 5a). We interpret this as a high-angle contact to the south and a lower-angled contact to the north; *Snavely and Wagner* [1982] also concluded that the Siletz-accretionary contact is low angle (25°) north of Willapa Bay. North of Grays Harbor, the higher velocities of the Siletz terrane are evident wrapping around the Olympic Mountains uplift. Correspondence between the surface outcrops of the Siletz terrane and the high-velocity anomalies at depth suggests a high-angle Siletz-accretionary prism contact in the shallowmost crust.

The alternating pattern of high and low velocities we observe along the coast (Plate 5a) may be the result of regional north-south directed compression [e.g., *McCrory*, 1996] that causes folding, variable thinning, and imbrication of the Siletz terrane. We suggest that regional north-south compression has domed the Siletz terrane south of Grays Harbor and in the Olympic Mountains along roughly east-west axes and has created an intervening synform. The relatively low velocities associated with the southern Grays Harbor region correspond with the Chehalis basin and imply that the basin is deep and has only a thin veneer of Crescent Formation near the surface; north of Grays Harbor, the low velocities may indicate that the Crescent Formation is downwarped. Relatively low velocities also coincide with the accreted sedimentary core of the anticlinal Olympic Mountains uplift [e.g., *Tabor and Cady*, 1978a].

The eastern edge of the Siletz terrane is more poorly constrained by our model; high-velocity rocks appear to be absent beneath the 1991 refraction profile at 7.5 km depth, where 5.0 km/s velocities are observed. *Miller et al*. [1997] analyzed the complete 1991 line and show velocities consistent with Siletz terrane at greater depth. *Moran* [1997] conducted a 3-D inversion using local earthquake sources centered east of Puget Sound and found a prominent north-south trending velocity boundary 50 km east of Puget Sound beginning at ~10 km

depth, which was interpreted as the east edge of the Siletz terrane.

2.5.2. The 12.5 km depth. The contact between accreted sedimentary rocks and the Siletz terrane makes a northeast trending boundary that occurs somewhat farther inland than it did at 7.5 km depth (Plate 6a). Missing at this depth are the alternating high- and low-velocity patterns evident at 7.5 km depth. In the southern Olympic Mountains and at Willapa Bay, significant northeast shifts in the terrane boundary with increasing depth can be seen by comparing its location at the surface and at depth (Plates 6a and 9). We interpret these shifts as evidence for a thin west edge of the Siletz terrane or shallow crustal faults that offset the surface outcrops of Siletz terrane from their deeper roots in the depth range between 7.5 and 12.5 km. In an inversion centered in the Puget Sound region, *Lees and Crosson* [1990] measured an 18° to 28° dip on this contact near the eastern Olympic Mountains, comparable to that imaged by *Clowes et al*. [1987] and *Calvert* [1996] at southern Vancouver Island. An interpretation of magnetotelluric data shows that the accreted sedimentary rocks do not underthrust the Siletz block at depths greater than ~10 km beneath Puget Sound [*Aprea et al*., 1998].

The low-velocity anomaly at Grays Harbor persists to 12.5 km depth (Plate 6a); the uniform velocities from the accretionary prism to the onshore parts of this area may imply that accretionary rocks were pushed onshore in similar fashion as to the north beneath the Olympic Mountains. To the east, high velocities drop off dramatically along a north trending boundary that corresponds roughly to the west Rainier seismic zone, consistent with previous interpretations that the deformation is occurring along the Siletzia boundary based on gravity interpretations [*Finn*, 1990; *Stanley et al*., 1996].

2.5.3. The 17.5 km depth. The primary change between 12.5 and 17.5 km depth is the observation of high-velocity rocks in the offshore region. We interpret these higher velocities as oceanic crust of the downgoing Juan de Fuca slab. Velocities appropriate for accretionary rocks make a nearly continuous linear boundary along the western edge of the Siletz terrane. A possible explanation for this may be that the compressional deformation (folding or faulting) of Siletzia is more pronounced at shallower depths. The north trending eastern boundary also persists at 17.5 km depth, consistent with a high-angle boundary.

2.5.4. The 22.5 km depth. At this depth we do not resolve the northeast trending lateral velocity contrast as observed from 2.5 to 17.5 km depth. We interpret this change as an indication that the base of the Siletz terrane occurs near this depth (to within ±5 km). The apparent 18–28 km thickness we model is in reasonable agreement with the estimates made from 2-D profiles [e.g., *Tréhu et al*., 1994; *Parsons et al*., 1998]. This depth coincides with a horizontal band of seismicity beneath Puget Sound [e.g., *Stanley et al*., 1996] and might imply that there is some deformation along the base of the Siletz terrane.

3. Discussion and Conclusions

We have imaged in 3-D the large-scale boundaries between the Siletz terrane and the adjacent accretionary prism and volcanic arc in western Washington. Internal deformation in Siletzia that manifests as alternating thinning and thickening along the Washington coast (Plate 5a) may result from folding and imbrication of the Siletz block on low-angle faults in the shallow crust (Plate 9). We observe the thick Siletz terrane of Oregon [*Tréhu et al*., 1994] persisting near the coast as far north as southern Willapa Bay. North of Willapa Bay at the latitude of Grays Harbor, the west edge of the Siletz terrane is thinned and has a lower-angled contact with the accretionary prism (Plate 9). This is consistent with deformation of the Crescent Formation basalt along the coast where it is exposed in seaward vergent overturned anticlines in the hanging walls of landward dipping thrust faults [e.g., *Snavely and Wagner*, 1982; *Wells and Coe*, 1985]. Seismic models from east of the Olympic Mountains and on Vancouver Island also show shallow easterly dips of the Siletz terrane in the upper 10 km with accretionary rocks beneath it [e.g., *Symons and Crosson*, 1997; *Lees and Crosson*, 1990; *Clowes et al*., 1987; *Calvert*, 1996], and *Pratt et al*. [1997] suggest a low-angle detachment beneath Puget Sound between 14 and 20 km depth. Therefore either the western edge of Siletzia was originally thinner at Willapa Bay and in the Olympic Mountains and is thus more susceptible to deformation or the more intense deformation in the northern Coast Ranges has involved Siletzia in low-angle faulting.

There is a high-amplitude antiformal uplift centered in the Olympic Mountains, and it appears that similar (but lower amplitude) deformation extends along much of the Washington margin with uplift between Willapa Bay and Grays Harbor, and synforms along the Columbia River and between Grays Harbor and the Olympic Mountains. Outside of our study area north of the Olympic Mountains, this pattern persists with a synformal structure that coincides with the Strait of Juan de Fuca [e.g., *Snavely*, 1987] (Figure 5). The Bouguer gravity anomaly associated with the Siletz terrane also reflects this pattern, with a coherent gravity high along the Oregon coast that grades into a more complex alternating pattern of highs and lows in Washington [*Finn et al*., 1991].

The shape of the western edge of the Siletz terrane in Washington may have implications for the geologic evolution of the margin. In Oregon, there is clear paleomagnetic evidence of clockwise rotation of the Siletz terrane [e.g., *Simpson and Cox*, 1977]. However, to the north on the Olympic Peninsula, the

Plate 9. (opposite) The 3-D velocity model for coastal Washington shown with the topography and generalized geology from Plate 3 draped above. (a) Cross section showing the western Siletz-accretionary terrane boundary at the coast of northern Oregon; basalt is present in the well indicated offshore, and we thus interpret a high-angle terrane contact. The eastern edge of Siletzia is poorly constrained in this cross section. (b) Basalt is observed in the well marked at the coast in this cross section; however, the main high-velocity anomaly is shifted to the east as compared with the northern Oregon section. We show a 25° dipping boundary after *Snavely and Wagner* [1982], who derived it from well data, shallow seismic reflection data, and magnetic modeling. Farther inland a well finds basalt at 2 km depth west of the Doty fault, which thrusts Siletzia rocks back to the surface [e.g., *Snavely and Wagner*, 1982; *Wells and Coe*, 1985]. We interpret a high-angle eastern boundary between Siletzia and the Cascade arc, coincident with the west Rainier seismic zone [e.g., *Stanley et al*., 1996; *Moran*, 1997]. (c) The Siletz terrane can be seen beneath the southern rim of the Olympic Mountains; we approximate a 25° dipping boundary between Siletzia and the underthrust accretionary complex. (d) Nearer to the axis of the Olympic Mountains uplift the Siletz terrane is bent sharply upward west of Puget Sound, where most of its thickness is exposed at the surface [e.g., *Tabor and Cady*, 1987a].

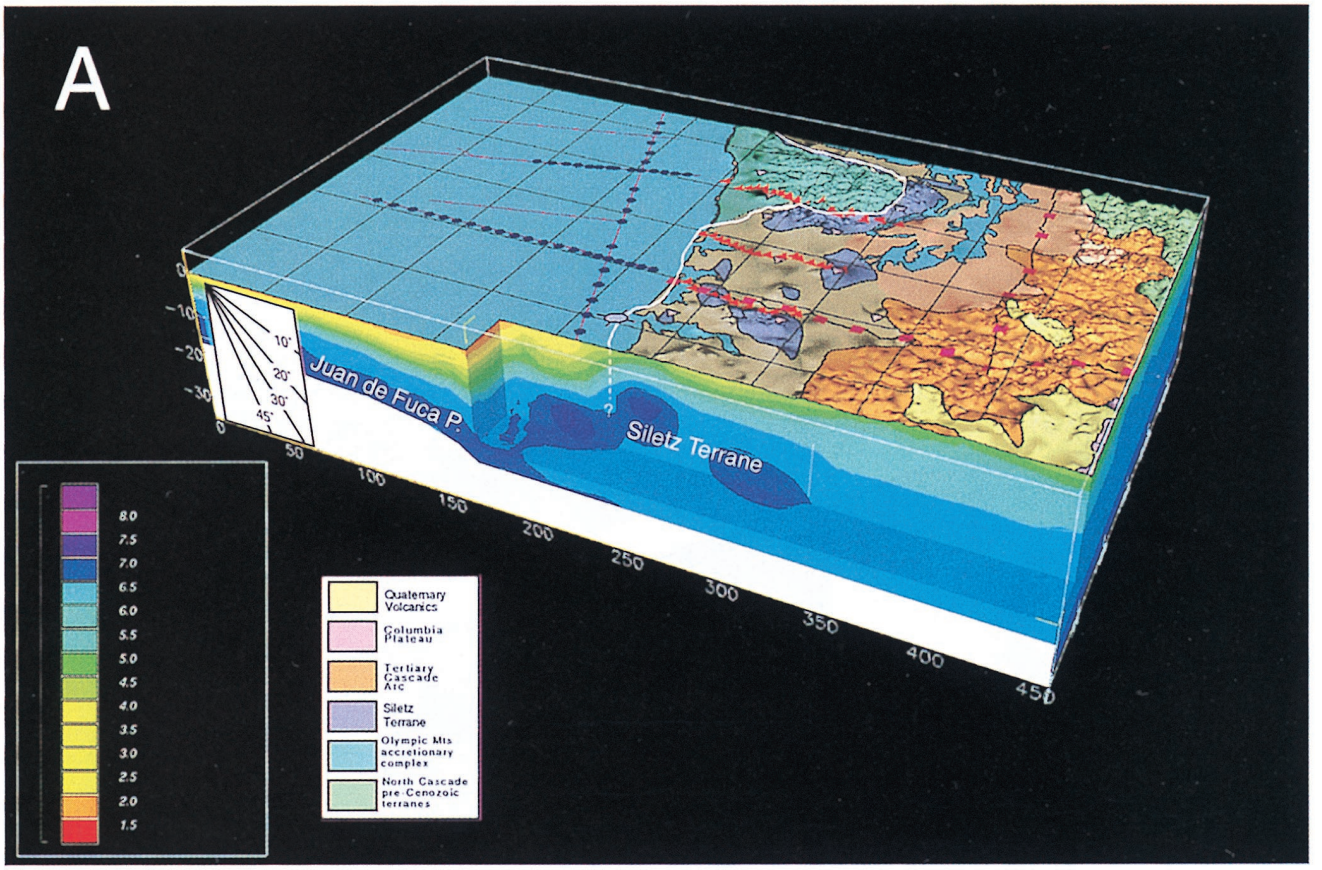
A
10°
20°
30°
45°
Juan de Fuca P.
Siletz Terrane
?
0
50
100
150
200
250
300
350
400
450
8.0
7.5
7.0
6.5
6.0
5.5
5.0
4.5
4.0
3.5
3.0
2.5
2.0
1.5
Quaternary Volcanics
Columbia Plateau
Tertiary Cascade Arc
Siletz Terrane
Olympic Mts accretionary complex
North Cascade pre-Cenozoic terranes

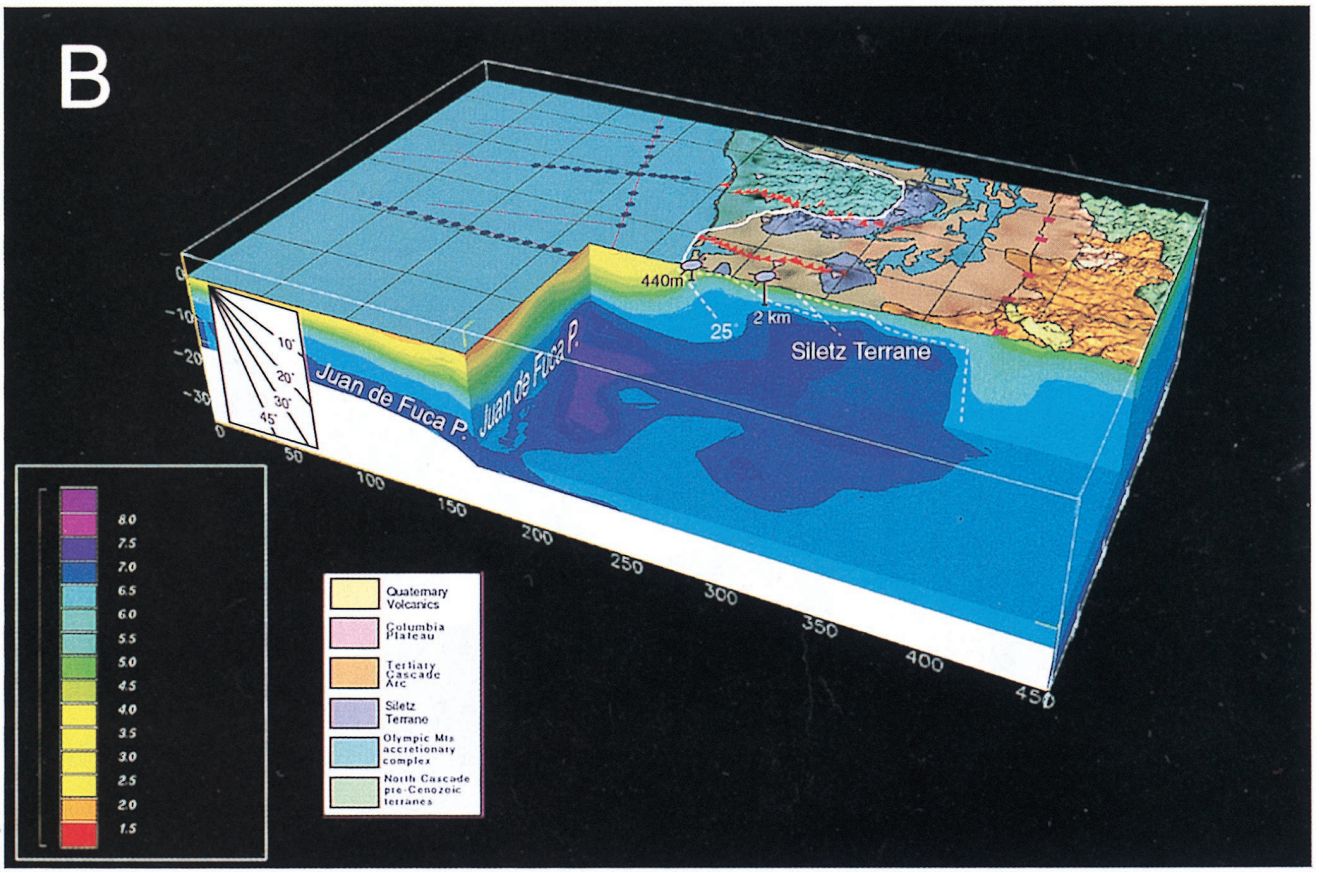
B
10°
20°
30°
45°
440m
25°
2 km
Juan de Fuca P.
Juan de Fuca P.
Siletz Terrane
0
50
100
150
200
250
300
350
400
450
8.0
7.5
7.0
6.5
6.0
5.5
5.0
4.5
4.0
3.5
3.0
2.5
2.0
1.5
Quaternary Volcanics
Columbia Plateau
Tertiary Cascade Arc
Siletz Terrane
Olympic Mts accretionary complex
North Cascade pre-Cenozoic terranes

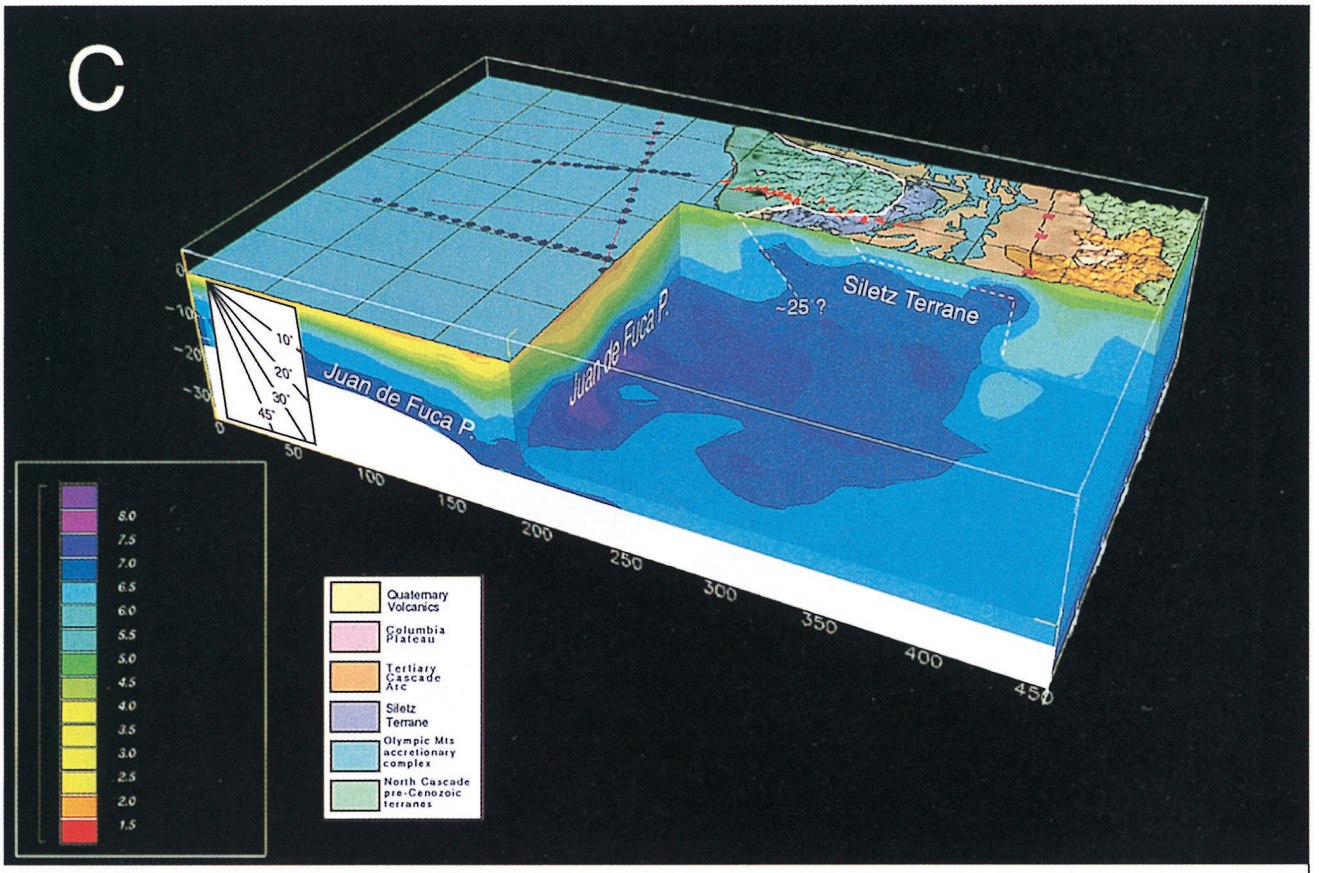

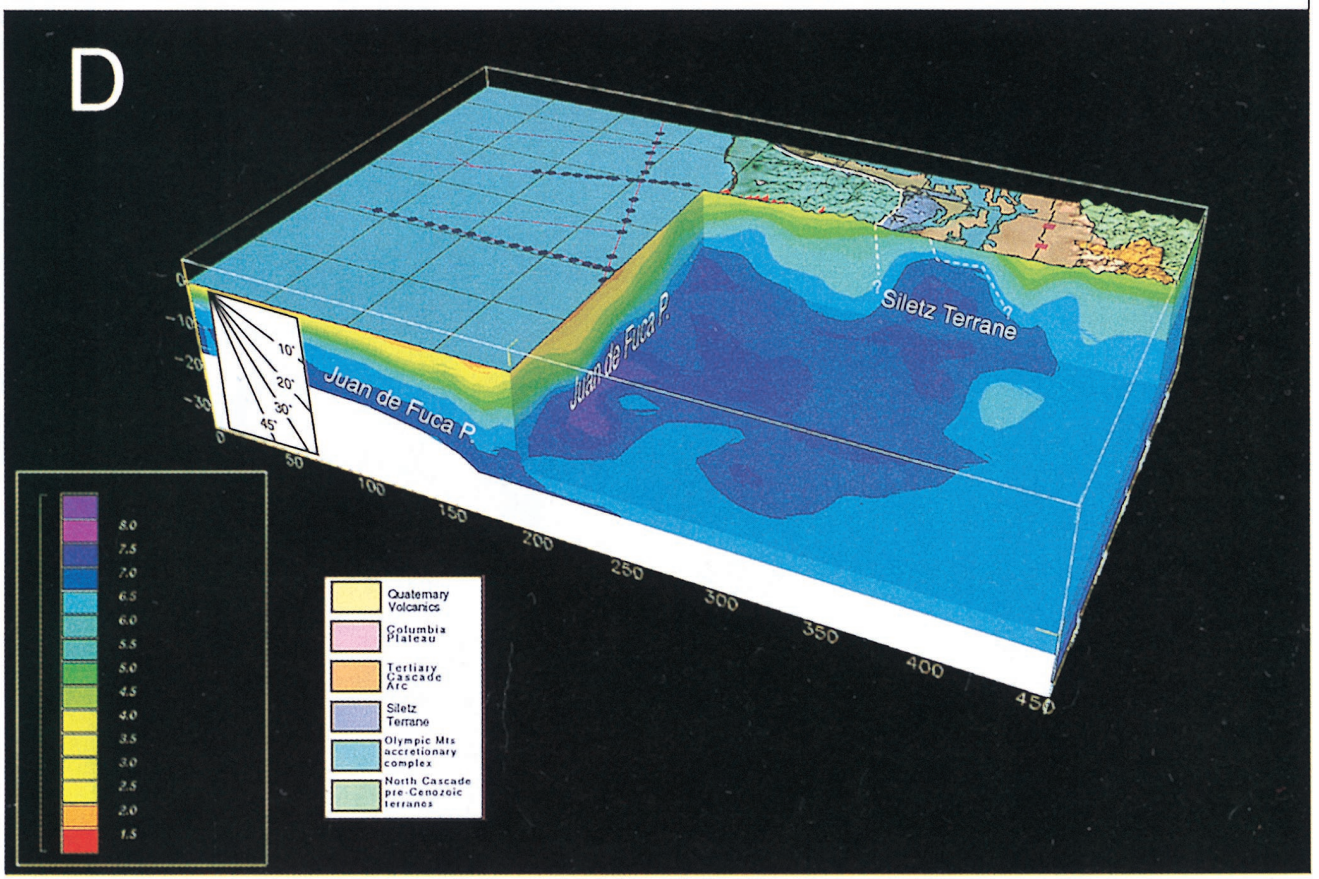

Plate 9. (continued)

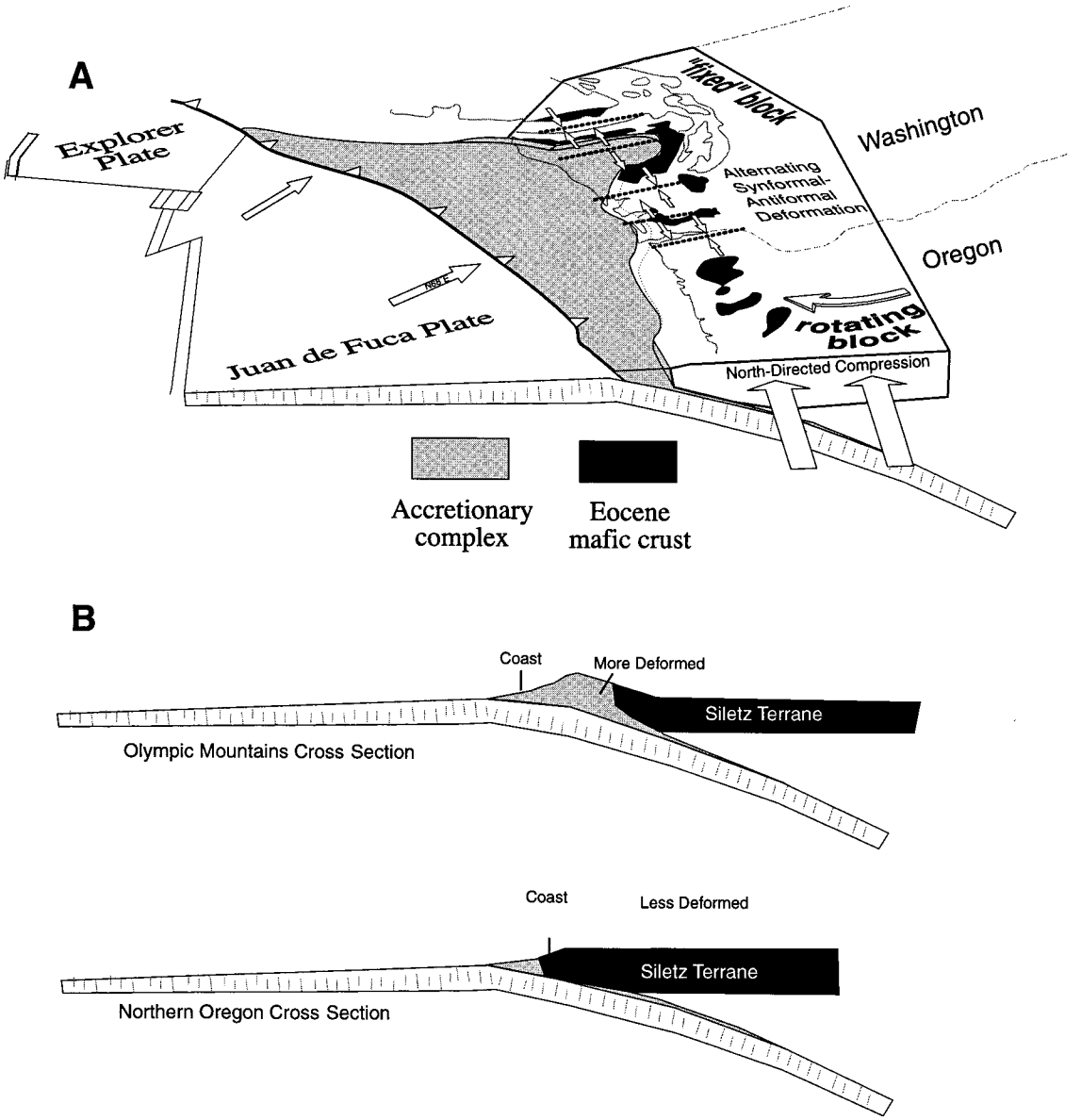

Figure 5. Tectonic model of Siletz-terrane deformation. (a) North directed compressional stress and southern Siletz terrane rotation are accommodated at a hinge point along the coast of the Olympic Peninsula. The greatest amplitude of uplift occurs at the Olympic Mountains, but the pattern of folding persists north and south of the Olympics. We suggest this occurs as a result of the margin-parallel northward transport and rotation of Siletzia into the relatively fixed restraining bend of the Canadian Coast Mountains at Vancouver Island. (b) Comparative cross sections through northern Oregon and the Olympic Mountains indicate the relationship between backstop deformation and sedimentary accretion, though whether this relationship is causative remains an open question.

Crescent Formation shows no rotation or translation [*Warnock et al.*, 1993]. Thus Siletzia must have accommodated this variable motion by internal deformation. Northwest directed translation of central Oregon and southern Washington [e.g., *Pezzopane and Weldon*, 1993] must also have been accommodated. We suggest that the internal strain of the Siletz terrane is focused along the coast of the Olympic Peninsula. The large-scale arching of the mafic basement along east-west trends transverse to the margin can be explained by margin-parallel northward transport and rotation of Siletzia into the relatively fixed restraining bend of the Canadian Coast Mountains at Vancouver Island [e.g., *Wells et al.*, 1998]. The Olympic Peninsula acted as a soft hinge point, undergoing significant north-south directed deformation. Alternatively, the size of the accretionary complex reflects proximity to the major proto-Columbia River sediment source [e.g., *Brandon and Vance*, 1992]. The deformation of Siletzia in Washington then represents the impact of major sediment accretion and possible tectonic erosion of the Crescent Formation along the thrust that locally forms its base in the Olympic Mountains [*Tabor and Cady*, 1978a].

The Siletz terrane acts as a backstop against which accreted rocks are thrust, and this contact may have seismogenic potential. We have provided a 3-D map of the contact zone at depth

that shows a fairly steep angle in northern Oregon and southernmost Washington. To the north, it appears that the Siletz backstop deforms along with the rocks accreted to it and may have active internal low-angle faults. North of Willapa Bay and in the western Olympic Mountains, the seaward edge of Siletzia appears to be a gently landward dipping thrust flake overlying imbricated and underthrust sediments of the Cascadia accretionary prism.

Acknowledgments. This work was supported by the German Ministry of Education, Research, Science, and Technology, the National Earthquake Hazards Reduction Program, and the USGS Continental Surveys and Coastal and Marine Geology Programs. We thank Bob Crosson, Ruth Ludwin, and Steve Malone at the University of Washington for helping us with arrival time data from the Pacific Northwest Seismic Network. Reftek seismographs were provided by the IRIS-PASSCAL instrument center at Stanford University; we thank Marcos Alvarez and Anthony Wei for their support during the controlled-source experiments. An early draft of this manuscript was improved by a review from Anne Tréhu. We thank Kate Miller, an anonymous reviewer and Associate Editor Alan Levander for their reviews.

References

Aprea, C., M. Unsworth, and J. Booker, Resistivity structure of the Olympic Mountains and Puget Lowlands, *Geophys. Res. Lett*., *25*, 109–112, 1998.

Atwater, B. F., Geologic evidence for earthquakes during the past 2000 years along the Copalis River, southern coastal Washington, *J. Geophys. Res*., *97*, 1901–1919, 1996.

Babcock, R. S., R. F. Burmester, D. C. Engebretson, and A. Warnock, A rifted margin origin for the Crescent basalts and related rocks in the northern coast range volcanic province, Washington and British Columbia, *J. Geophys. Res*., *97*, 6799–6821, 1992.

Beck, M. E., Jr., and C. D. Burr, Paleomagnetism and tectonic significance of the Goble volcanic series, southwestern Washington, *Geology*, *7*, 175–179, 1979.

Best, M. G., *Igneous and Metamorphic Petrology*, 630 pp., W. H. Freeman, New York, 1982.

Blackwell, D. D., J. L. Steele, and S. Kelley, Heat flow in the state of Washington and thermal conditions in the Cascade Range, *J. Geophys. Res*., *95*, 19,495–19,516, 1990.

Brandon, M. T., and A. R. Calderwood, High-pressure metamorphism and uplift of the Olympic subduction complex, *Geology*, *18*, 1252–1255, 1990.

Brandon, M. T., and J. A. Vance, Tectonic evolution of the Cenozoic Olympic subduction complex, Washington State, as deduced from zircon fission track ages for detrital zircons, *Am. J. Sci*., *292*, 565–636, 1992.

Calvert, A. J., Seismic reflection constraints on imbrication and underplating of the northern Cascadia margin, *Can. J. Earth Sci*., *33*, 1294–1307, 1996.

Christensen, N. I., and W. D. Mooney, Seismic velocity structure and composition of the continental crust: A global view, *J. Geophys. Res*., *100*, 9761–9788, 1995.

Clowes, R. M., M. T. Brandon, A. G. Green, C. J. Yorath, A. S. Sutherland, E. R. Kanesewich, and C. Spencer, LITHOPROBE—Southern Vancouver Island: Cenozoic subduction complex imaged by deep seismic reflections, *Can. J. Earth Sci*., *24*, 31–51, 1987.

Crosson, R. S., and T. J. Owens, Slab geometry of the Cascadia subduction zone beneath Washington from earthquake hypocenters and teleseismic converted waves, *Geophys. Res. Lett*., *14*, 824–827, 1987.

DeMets, C. R. G. Gordon, D. F. Argus, and S. Stein, Current plate motions, *Geophys. J. Int*., *101*, 425–478, 1990.

Dewey, J. W., D. P. Hill, W. L. Ellsworth, and E. R. Engdahl, Earthquakes, faults, and the seismotectonic framework of the contiguous United States, in *Geophysical Framework of the Continental United States* edited by L. C. Pakiser, and W. D. Mooney, *Mem. Geol. Soc. Am*., *172*, 541–576, 1989.

Duncan, R. A., A captured island arc chain in the Coast Range of Oregon and Washington, *J. Geophys. Res*., *87*, 10,827–10,837, 1982.

Finn, C., Geophysical constraints on Washington convergent margin structure, *J. Geophys. Res*., *95*, 19,533–19,546, 1990.

Finn, C., W. M. Phillips, and D. L. Williams, Gravity and terrane maps of Washington, *U.S. Geol. Surv. Geophys. Invest. Map*, *GP-988*, scale 1:125,000, 1991.

Flueh, E., M. Fisher, D. Scholl, T. Parsons, U. ten Brink, D. Klaeschen, N. Kukowski, A. Tréhu, J. Childs, J. Bialas, and N. Vidal, Scientific teams analyze earthquake hazards of the Cascadia subduction zone, *Eos Trans. AGU*, 153–157, 1997.

Heaton, T. H., and S. H. Hartzell, Earthquake hazards on the Cascadia subduction zone, *Science*, *236*, 162–168, 1987.

Heaton, T. H., and H. Kanamori, Seismic potential associated with subduction in the northwestern United States, *Bull. Seismol. Soc. Am*., *74*, 933–941, 1984.

Hole, J. A., Nonlinear high-resolution three-dimensional seismic travel time tomography, *J. Geophys. Res*., *97*, 6553–6562, 1992.

Hole, J. A., and B. C. Zelt, 3-D finite-difference reflection traveltimes, *Geophys. J. Int*., *121*, 427–434, 1995.

Humphreys, E., and R. W. Clayton, Adaptation of back projection tomography to seismic travel time problems, *J. Geophys. Res*., *93*, 1073–1085, 1988.

Irving, E., Paleopoles and paleolatitudes of North America and speculations about displaced terranes, *Can. J. Earth Sci*., *16*, 669–694, 1979.

Lees, J. M., and R. S. Crosson, Tomographic imaging of local earthquake delay times for three-dimensional velocity variation in western Washington, *J. Geophys. Res*., *95*, 4763–4776, 1990.

Magill, J., A. Cox, and R. Duncan, Tillamook volcanic series: Further evidence for tectonic rotation of the Oregon Coast Range, *J. Geophys. Res*., *86*, 2953–2970, 1981.

Massey, N. W. D., Metchosin igneous complex, southern Vancouver Island: Ophiolite stratigraphy developed in an emergent island setting, *Geology*, *14*, 602–605, 1986.

McCrory, P. A., Tectonic model explaining divergent contraction directions along the Cascadia subduction margin, Washington, *Geology*, *24*, 929–932, 1996.

McFarland, C. R., Oil and gas exploration in Washington, *Inf. Cir. Wash. Div. Geol. Earth Resour*., *67*, 119 pp., 1979.

Michaelson, C. A., and C. S. Weaver, Upper mantle structure from teleseismic *P* wave arrivals in Washington and northern Oregon, *J. Geophys. Res*., *91*, 2077–2094, 1986.

Miller, K. C., G. R. Keller, J. M. Gridley, J. H. Luetgert, W. D. Mooney, and H. Thybo, Crustal structure along the flank of the Cascades, western Washington, *J. Geophys. Res*., *102*, 17,857–17,873, 1997.

Moran, S. C., Three-dimensional *P*-wave velocity structure in the greater Mount Rainier area from local earthquake tomography, Ph.D. thesis, 167 pp., Univ. of Wash., Seattle, 1997.

Parsons, T., A. M. Tréhu, J. H. Luetgert, K. Miller, F. Killbride, R. E. Wells, M. A. Fisher, E. Flueh, U. S. ten Brink, and N. I. Christensen, A new view into the Cascadia subduction zone and volcanic arc: Implications for earthquake hazards along the Washington margin, *Geology*, *26*, 199–202, 1998.

Pezzopane, S. K., and R. J. Weldon, Tectonic role of active faulting in central Oregon, *Tectonics*, *12*, 1140–1169, 1993.

Pratt, T. L., S. Johnson, C. Potter, W. Stephenson, and C. Finn, Seismic reflection images beneath Puget Sound, western Washington State: The Puget Lowland thrust sheet hypothesis, *J. Geophys. Res*., *102*, 27,469–27,489, 1997.

Shaw, P. R., and J. A. Orcutt, Waveform inversion of seismic refraction data and applications to young Pacific crust, Geophys. *J. R. Astron. Soc*., *82*, 375–414, 1986.

Simpson, R. W., and A. Cox, Paleomagnetic evidence for tectonic rotation of the Oregon Coast Range, *Geology*, *5*, 585–589, 1977.

Snavely, P. D., Tertiary geologic framework, neotectonics, and petroleum potential of the Oregon-Washington continental margin, in *Geology and Resource Potential of the Continental Margin of Western North America and Adjacent Ocean Basins—Beaufort Sea to Baja California*, *Earth Sci. Ser*., vol. 6, edited by D. W. Scholl, A. Grantz, and J. G. Vedder, pp. 305–335, Circum-Pac. Counc. for Energy and Miner. Resour., Houston, Tex., 1987.

Snavely, P. D., Jr., and H. C. Wagner, Geologic cross-section across the continental margin of southwestern Washington, *U.S. Geol. Surv. Open File Rep*., 82-459, 10 pp., 1982.

Snavely, P. D., Jr., and R. E. Wells, Cenozoic evolution of the continental margin of Oregon and Washington, in *Assessing Earthquake*

Hazards and Reducing Risk in the Pacific Northwest, edited by A. M. Rogers et al., *U.S. Geol. Surv. Prof. Pap*., *1560*, 161–182, 1996.

Snavely, P. D., N. S. MacLeod, and H. C. Wagner, Tholeiitic and alkalic basalts of the Eocene Siletz River volcanics, Oregon Coast Range, *Am. J. Sci*., *266*, 454–481, 1968.

Stanley, W. D., S. Y. Johnson, A. I. Qamar, C. S. Weaver, and J. M. Williams, Tectonics and seismicity of the southern Washington Cascade Range, *Bull. Seismol. Soc. Am*., *86*, 1–18, 1996.

Symons, N. P., and R. S. Crosson, Seismic velocity structure of the Puget Sound region from 3-D non-linear tomography, *Geophys. Res. Lett*., *24*, 2593–2596, 1997.

Tabor, J. J., and B. T. R. Lewis, Crustal structure of the Washington continental margin from refraction data, *Bull. Seismol. Soc. Am*., *76*, 1011–1024, 1986.

Tabor, R. W., and W. M. Cady, The structure of the Olympic Mountains, Washington—Analysis of a subduction zone, *U.S. Geol. Surv. Prof. Pap*., *1033*, 38 pp., 1978a.

Tabor, R. W., and W. M. Cady, Geologic map of the Olympic Peninsula, Washington, *U.S. Geol. Surv. Misc. Invest. Ser*., *Map I-994*, 1978b.

Thurber, C. H., Local earthquake tomography: Velocities and *Vp*/*Vs*—Theory, in *Seismic Tomography: Theory and Practice*, pp. 663–683, edited by H. M. Iyer and K. Hirahara, Chapman and Hall, New York, 1993.

Tréhu, A. M., I. Asudeh, T. M. Brocher, J. Luetgert, W. D. Mooney, J. L. Nabelek, and Y. Nakamura, Crustal architecture of the Cascadia forearc, *Science*, *266*, 237–243, 1994.

Vidale, J. E., Finite-difference calculation of traveltimes in three dimensions, *Geophysics*, *55*, 521–526, 1990.

Warnock, A. C., R. F. Burmeister, and D. C. Engebretson, Paleomagnetism and tectonics of the Crescent formation, northern Olympic Mountains, *J. Geophys. Res*., *98*, 11,729–11,742, 1993.

Wells, R. E., and R. S. Coe, Paleomagnetism and geology of Eocene volcanic rocks of southwest Washington: Implications for mechanisms of tectonic rotation, *J. Geophys. Res*., *90*, 1925–1947, 1985.

Wells, R. E., and C. S. Weaver, Cenozoic deformation of Pacific Northwest coastal regions, in *Proceedings of the National Earthquake Prediction Evaluation Council*, edited by V. A. Frizzell, *U.S. Geol. Surv. Open File Rep*., *93-333*, 14–16, 1993.

Wells, R. E., D. C. Engebretson, P. D. Snavely Jr., and R. S. Coe, Cenozoic plate motions and the volcano-tectonic evolution of western Oregon and Washington, *Tectonics*, *3*, 275–294, 1984.

Wells, R. E., C. S. Weaver, and R. J. Blakely, Fore arc migration in Cascadia and its neotectonic significance, *Geology*, *26*, 759–762, 1998.

M. A. Fisher, T. Parsons, and R. E. Wells, U.S. Geological Survey, MS 999, 345 Middlefield Road, Menlo Park, CA 94025. (tparsons@usgs.gov)

E. Flueh, GEOMAR Research Center for Marine Geosciences, Wischhofstr. 1-3, D-24148 Kiel, Germany.

U. ten Brink, U.S. Geological Survey, Quissett Campus, 384 Woods Hole Road, Woods Hole, MA 02543.

(Received April 17, 1998; revised November 5, 1998;
accepted March 10, 1999.)